Fall 2009

Filtering, modeling, and control of axial force signals in friction stir welding processes

Thomas Michael Oakes

Department:

FILTERING, MODELING, AND CONTROL OF AXIAL FORCE SIGNALS IN FRICTION STIR WELDING PROCESSES

by

THOMAS MICHAEL OAKES

A THESIS

Presented to the Faculty of the Graduate School of the

MISSOURI UNIVERSITY OF SCIENCE AND TECHNOLOGY

In Partial Fulfillment of the Requirements for the Degree

MASTER OF SCIENCE
IN MECHANICAL ENGINEERING

2009

Approved by

R. G. Landers Advisor
M. C. Leu
R. S. Mishra

PUBLICATION THESIS OPTION

This thesis consists of the following two articles that have been submitted for publication as follows:

Pages 3-38 are intended for submission as a chapter for KALMAN FILTER: RECENT ADVANCES AND APPLICATIONS

Pages 37-56 are intended for submission in AMERICAN CONTROLS CONFERENCE 2009

ABSTRACT

In Friction Stir Welding Processes, good contact between tool and work piece can be accomplished through control of the axial force signals. A method of stochastic modeling is introduced and used in conjunction with a Kalman filter to develop empirical static and dynamic models relating the axial force to input process parameters. The filtering method reduces signal variance by an order of magnitude. The models are experimentally validated and used to design and implement a general tracking controller with disturbance rejection for axial force control. Online control of the axial force is experimentally validated for bead-on-plate welds using a 6061 aluminum alloy for constant and sinusoidal axial force reference signals.

ACKNOWLEDGMENTS

I would like to thank my advisor, Dr. R. G. Landers for the opportunity to work with him on this project. Especially for all the time, support, advice, understanding, and funding he provided to help me get this far. I couldn't have chosen a better advisor. I would also like to thank Dr. M. C. Leu and Dr. R. S. Mishra for their funding, support, and participation on my graduate committee.

Special thanks to my parents for putting up with my stubbornness this past year. I couldn't have got this far without you.

TABLE OF CONTENTS

LIST OF ILLUSTRATIONS

Figure Page

PAPER 1

LIST OF TABLES

SECTION

1. INTRODUCTION

Measurements from most manufacturing processes contain significant variation due to both electrical and process noise which can hinder process modeling and controller implementation. The Kalman filter is a model-based optimal filter that compares a system model and measurement signal with weighted certainties to determine the optimal estimate. While first principle models are ideal for this type of estimation, they seldom exist for most types of manufacturing processes due to the inherent nonlinearities.

Empirical methods of model identification are used to approximate the process dynamics through reconstruction of the known inputs and signal measurements. These dynamics are sensitive to variations in the signal, implying the necessity for signal processing prior to process modeling. The same signals are often used for process control and can cause wear on the actuator due to noise frequencies that exceed the actuator bandwidth.

Chapter two contains a paper published as a book chapter in "Kalman Filter: Recent Advances and Applications", published in 2009. It introduces a method of stochastically modeling manufacturing processes as first order for use with a Kalman Filter. The Filtering Methodology is discussed and applied to examples in Friction Stir Welding and Laser Metal Deposition.

Friction Stir Welding (FSW) is a solid state joining process invented in 1991 at the Welding Institute in Cambridge, United Kingdom. Unlike conventional fusion welding, FSW is capable of joining aluminum alloys as well as dissimilar materials without need for filler material. The technology boasts high energy efficiency, low shrinkage, and excellent weld strength.

The FSW process utilizes a tool consisting of a larger shoulder and smaller threaded pin region, often tapered with flats and/or flutes to enhance material mixing. The rotating, non – consumable tool is plunged into the work piece and the process reaches minimal operational depth as the pin is completely submerged and the shoulder comes into contact with the material surface. The tool dwells for a time as the friction

between the shoulder and work piece heat the material and the pin causes mixing and plastic deformation. The tool is then advanced along the weld path, joining materials due to an elevated temperature field caused by friction and plastic deformation. The work piece temperature does not exceed the material melting temperature, thus reducing the heat affected zone and providing good weld properties.

Three process parameters in FSW are the plunge depth, the traverse rate, and the spindle rotation speed. A significant amount of work has been done to model the FSW process with respect to these three input parameters for use in control and process optimization. It has been found that good weld quality is highly dependent on maintaining proper contact between the tool and work piece [1], and trends have been established relating defect generation and high path force measurements [2]. A study conducted by Zhao et al. [3] developed empirical models relating the input process parameters to both the path and axial forces. A later study conducted by the same authors used these models to design and test controllers to regulate the axial and path force signals [4].

Chapter three contains a paper published in the 2009 American Control Conference. The paper utilizes the filtering method introduced in chapter two for empirical modeling of the axial force signals of Friction Stir Welding processes with respect to the input process parameters. A general tracking controller with disturbance rejection is designed and implemented for control of the axial force by online manipulation of the plunge depth.

PAPER

1. KALMAN FILTERING FOR MANUFACTURING PROCESSES

Oakes, T., Tang, L., Landers, R. G., Balakrishnan, S. N.
Department of Mechanical and Aerospace Engineering
Missouri University of Science and Technology – Rolla, Missouri, U.S.A 65401
Email: tmo6w3@mst.edu, ltx8d@mst.edu, landersr@mst.edu, bala@mst.edu

ABSTRACT

Manufacturing process measurements are inherently noisy. While this is due, in part, to electrical noise, a significant portion of the noise is due to the manufacturing process itself. Even when constant process parameters are applied, measurements contain tremendous variation due to naturally occurring phenomena in the process. To utilize the process measurements to construct dynamic models and perform on–line control, the process measurements must be filtered to decrease this variation. Even the variation due to the manufacturing process must be properly filtered since the bandwidth of these variations is typically beyond the actuator's bandwidth. This chapter presents a methodology, based on stochastic modeling and Kalman filtering, to significantly reduce the variation in manufacturing process measurements. The methodology is applied to axial force measurements in a Friction Stir Welding (FSW) process and temperature measurements in a Laser Metal Deposition (LMD) process. The results demonstrate the methodology is able to accurately reproduce the measurements with a significant reduction in variation while preserving the measurement's phase and steady–state characteristics. The filtering methodology is utilized in the dynamic process modeling

and control of FSW and LMD processes. The results demonstrate that better models and process control are realized when utilizing the filtering methodology.

I. INTRODUCTION

Unwanted signal variation commonly occurs in manufacturing process measurements. This variation, due to both random electrical noise and noise in the manufacturing process itself, can be quantified by calculating the steady–state process data variance

$$\sigma^2 = \frac{1}{N}\left[\left(\sum_{i=1}^{N} x_i\right)^2 - \left(\sum_{i=1}^{N} \frac{x_i}{N}\right)^2\right] \tag{1}$$

where x_i is the measurement at iteration i and N is the number of samples. Noise due to the manufacturing process itself is often greater in magnitude than the electrical noise. Examples of process noise include: (1) high frequency cyclic variations due to tool eccentricity in a turning process, (2) low frequency variations due to discrete solidification of deposited material in Laser Metal Deposition (LMD) processes, and (3) chaotic mixing of materials in Friction Stir Welding (FSW) processes.

Manufacturing process measurements must be filtered before the data can be used for dynamic modeling or control. First principle modeling is generally unable to capture inherent nonlinear dynamics such as non–uniform friction and system wear. Also, first principle models do not always exist for certain aspects of manufacturing processes. For these reasons, dynamic manufacturing process models are often developed empirically. Estimation techniques such as Recursive Least Squares and Particle Swarm Optimization are commonly used for system identification to create a “best fit” model based on

collected measurements. However, the fidelity of an empirical model greatly depends upon the measurements used to create it and processes with high–magnitude variations in the measurement signals are often difficult to model due to the low signal–to–noise ratio. Manufacturing process models are often used to design process controllers. Process control is the on–line adjustment of process parameters to enhance operation productivity and improve part quality. Variations in the measurement signal are generally higher in frequency than the available actuator bandwidth, which can lead to increased actuator wear and possible stability issues. A filter must be developed for (1) post processing of data to compensate for large signal variations prior to use by a model identification method and (2) on–line filtering capable of preserving signal phase and offset with minimal computational burden.

The fourth order low pass Butterworth filter is used for a number of manufacturing processes. Bhattacharyya and Sengupta (2007) used a fourth order low pass Butterworth filter on a face milling process to remove high frequency variation due to spindle rotation harmonics. Liang et al. (2002) employed a Butterworth filter on the spindle power signal of an end milling process for use in a fuzzy logic controller. Ghosh et al. (2007) used a Butterworth filter for neural–based sensor fusion to estimate tool wear. Another common filter is a point–averaging filter. Freitag (2004) used a 50 ms Finite Impulse Response moving average filter to smooth command signals sent to the process controller of a miniature ball end mill. Zhao et al. (2007) employed a five point moving average filter to reduce the standard deviation of the axial force signal of a FSW process for the purpose of modeling and process control.

The objective of this chapter is to present a new method for filtering manufacturing process measurement signals via the use of a two–step Kalman filter. The rest of the chapter is organized as follows. A general filtering methodology is established that uses a stochastic model and a two–step Kalman filter. The filtering methodology is compared to other common filters and then applied to FSW and LMD processes. Post process filtering is performed on FSW and LMD processes to develop dynamic process models. On–line filtering is performed for FSW and LMD processes for use with process controllers.

II. FILTERING METHODOLOGY

Unlike standard frequency–based filters, the Kalman filter is a time domain filter that recursively estimates and updates process states using data from both a dynamic system model and collected measurements. Selection of a reliable dynamic process model is vital in maximizing the filter performance. A Markov process is a model that expresses the stochastic evolution of a system. This implies that knowledge of the present system states completely describes all relevant information necessary for the process evolution. Past and future states of a Markov Process are statistically independent. The excessive signal variation observed in many manufacturing processes leads to the realization that these processes can be modeled as Markov processes. A general stochastic model of a manufacturing process is

$$\dot{x}(t) = \lambda x(t) + w(t) \tag{2}$$

where $x(t)$ is the system state, λ is the system pole, and $w(t)$ is the process noise, which accounts for the system's stochastic nature, as well as changes in the input. It is assumed

the process noise is Gaussian with a zero mean normal distribution and variance, *Q*. Transforming equation (2) into the discrete–time domain using a zero order hold

$$x(k) = e^{\lambda T_s} x(k-1) + w(k-1) \tag{3}$$

where *k* is the time step and T_s is the sample period (s). The two–step discrete–time Kalman filter uses the model

$$x(k) = Fx(k-1) + Gu(k-1) + w(k-1) \tag{4}$$

where $F = e^{\lambda T_s}$ and *u*(*k*–1) = 0 to fit the form of equation (3). The input term in equation (4) is set to zero to allow the process noise term to account for all deviations in the state due to model uncertainty and input changes. Equation (4) has process noise characteristics

$$w \sim N(0, Q) \qquad E\left(w(k)\,w(k)^T\right) = Q \tag{5}$$

The measurement is

$$y(k) = Hx(k) + v(k) \tag{6}$$

Equation (6) has measurement noise characteristics

$$v \sim N(0, R) \qquad E\left(v(k)\,v(k)^T\right) = R \tag{7}$$

where *R* is the measurement variance. Initial values of the state estimate and covariance, respectively, are

$$\hat{x}^+(0) = x(0) \tag{8}$$

$$P^+(0) = E\left|\left(x(0) - \hat{x}^+(0)\right)\left(x(0) - \hat{x}^+(0)\right)^T\right| \tag{9}$$

where $\hat{x}^+$ is the state estimate after the filter's measurement update (aposteriori) and P^+ is the covariance after the filter's measurement update. A large initial covariance matrix is

required to ensure the estimates convergence. Equation (4) is rewritten in terms of its estimates

$$\hat{x}^{-}(k) = e^{\lambda T}\hat{x}^{+}(k-1) \tag{10}$$

where $\hat{x}^{-}$ is the state estimate before the filter's measurement update (apriori). Equation (10) is used to propagate the state estimate to the next time step. The covariance is propagated to the next time step using

$$P^{-}(k) = FP^{+}(k-1)F^{T} + Q \tag{11}$$

where P^{-} is the covariance prior to the filter's measurement update. The Kalman gain matrix is

$$K(k) = P^{-}(k)H^{T}\left[HP^{-}(k)H^{T} + R\right] \tag{12}$$

Then the measurement is used to update, respectively, the state estimate and covariance

$$\hat{x}^{+}(k) = \hat{x}^{-}(k) + K(k)\left[y(k) - H\hat{x}^{-}(k)\right] \tag{13}$$

$$P^{+}(k) = \left[I - K(k)H\right]P^{-}(k)\left[I - K(k)H\right]^{T} + K(k)RK^{T}(k) \tag{14}$$

The computations in equations (10)–(14) are repeated at each time step.

A. Filter Tuning

A generic first order system is used to illustrate the tuning required for the filtering methodology. The system's transfer function is

$$G(s) = \frac{K}{\tau s + 1} = \frac{6}{0.6s + 1} \tag{15}$$

where K is the gain and τ is the time constant. The system is converted into the discrete–time domain using a zero order hold and T_s = 0.01 s

$$G(z) = \frac{0.1}{z - 0.9835} \tag{16}$$

The unit step response is shown in Figure 1. Random noise with variance 0.25 is added to the output to simulate a noisy measurement. The measurement variance, *R*, is calculated directly from the measurement data while values of λ and *Q* are tuned to optimize the filter's performance. This can be accomplished by first setting *Q* equal to *R*, implying equal faith in the measurements and model, and tuning λ while leaving *Q* and *R* constant until the disparity between the filtered and measured data is minimized.

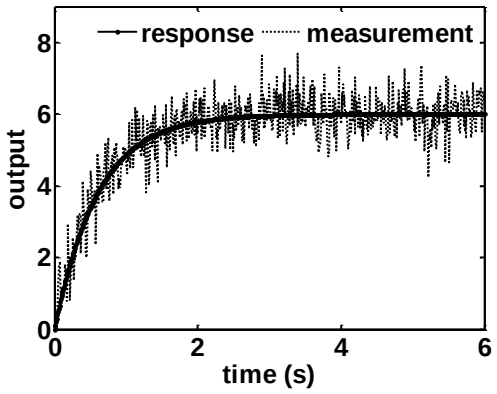

Figure 1. Unit step response of system described by equation (16).

Figure 2 illustrates the effect of tuning λ. As λ approaches zero, the observable offset between the measurement data and the estimated state is eliminated. For this particular portion of the tuning process, it can be assumed that the optimal value of λ is zero.

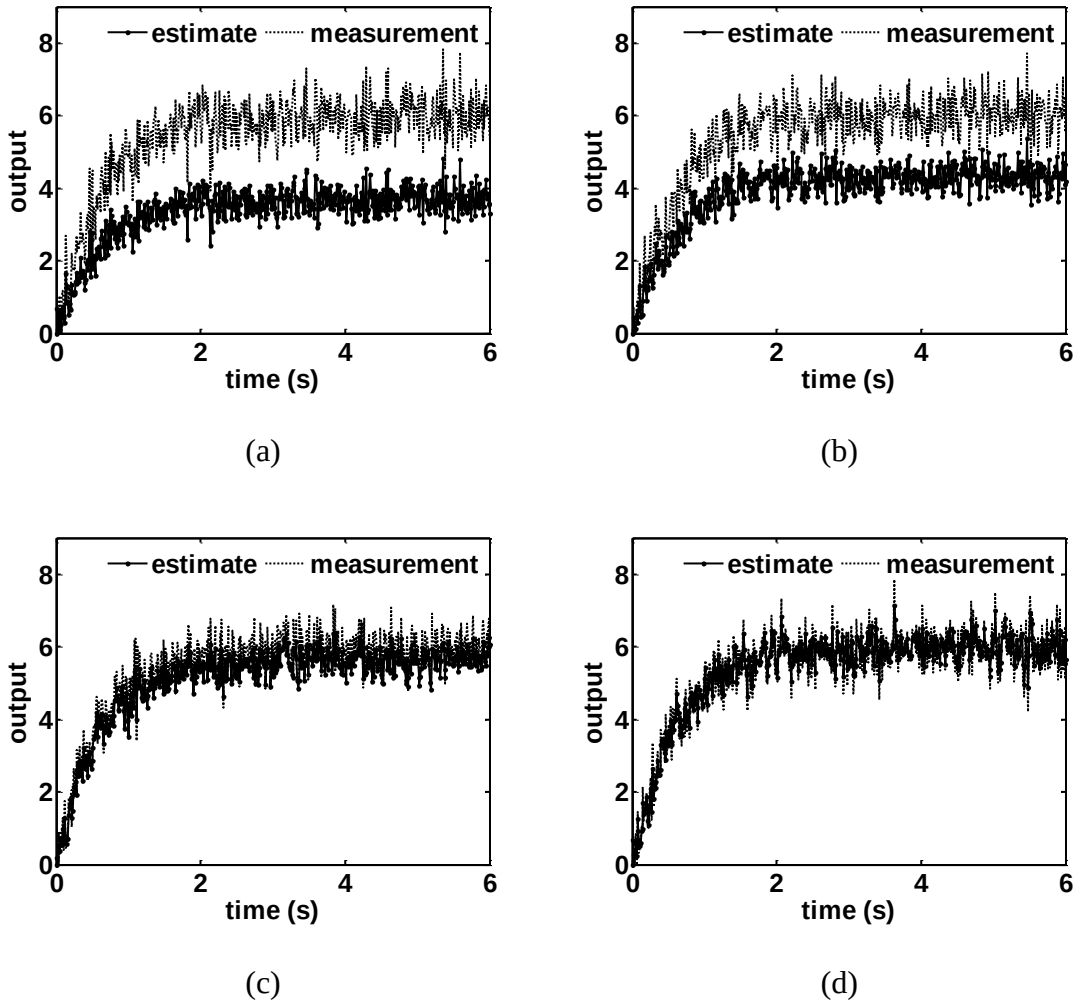

Figure 2. Outputs and estimates for unit step input for system described by equation (16) and different values of λ. (a) $\lambda = -1000$, (b) $\lambda = -100$, (c) $\lambda = -10$, and (d) $\lambda = 0$, with $Q = R = 0.25$ and $T_s = 0.01$ s.

After an appropriate value of λ is selected, Q is reduced with respect to R. Reduction of the signal variance is observed as faith in the model increases (i.e., as Q decreases), as shown in Figure 3. Figure 3c demonstrates the algorithm can be used to effectively reduce the signal variance by nearly an order of magnitude while preserving the phase. The parameter Q can be reduced to the point that an increased delay in the

filter's response time is observed as shown in Figure 3d. This can adversely affect modeling by making the system appear to have a slower response than its actual response. Despite the approximate 0.5 s time delay, the variance of the state estimate in Figure 3d is reduced by a factor of 50.

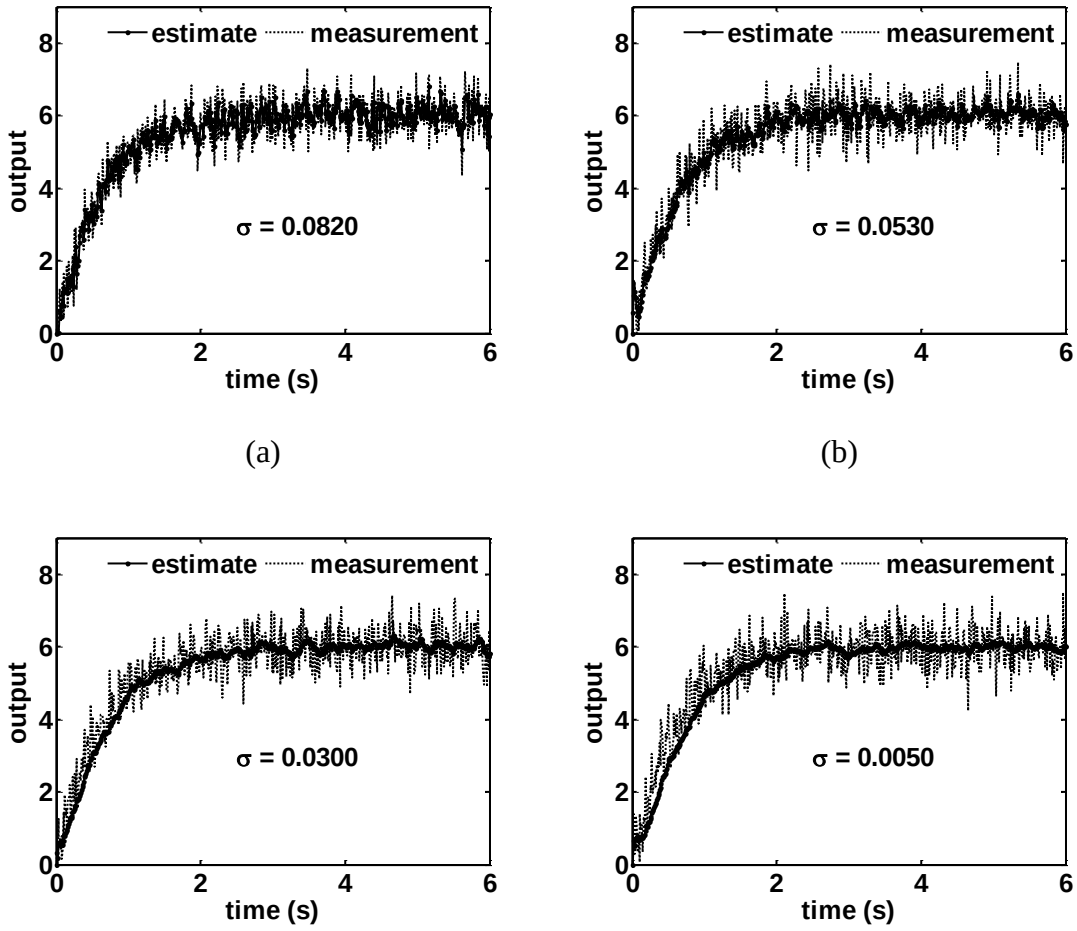

Figure 3. Outputs and estimates for unit step input for system described by equation (16) and different values of Q. (a) $Q = 0.5R$, (b) $Q = 0.1R$, (c) $Q = 0.01R$, and (d) $Q = 0.005R$, with $\lambda = 0$ and $T_s = 0.01$ s.

The sampling rate also has a tremendous affect on the tuning process and the filter performance. Applying a zero order hold to equation (15) with T_s = 0.1 s

$$G(z) = \frac{0.9288}{z - 0.8465} \tag{17}$$

With λ = 0, the same tuning process of Q is performed to illustrate the affect the sample rate has on the filter performance. The results are shown in Figure 4. The lower sampling rate present in Equation (17) impacts the degree to which adjusting the value of Q will affect the phase. Lowering the value of Q significantly reduces the variance when compared to Figure 3; however, it also significantly increases the phase offset due to less data being available to the filter during the transient portion of the process.

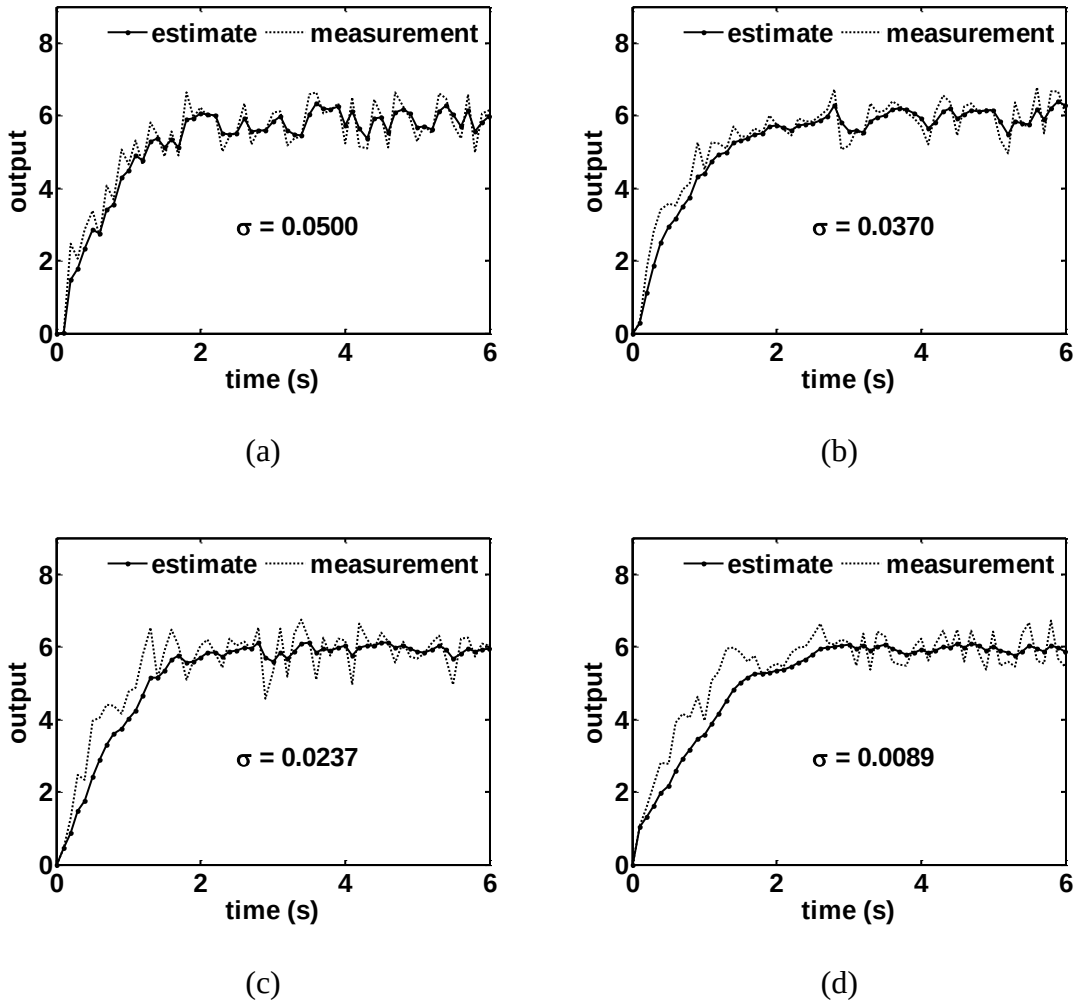

Figure 4. Outputs and estimates for unit step input for system described by equation (17) and different values of Q. (a) $Q = 0.5R$, (b) $Q = 0.25R$, (c) $Q = 0.1R$, and (d) $Q = 0.05R$, with $\lambda = 0$ and $T_s = 0.1$ s.

B. Filter Comparison

The performances of two common digital filters are compared to that of the proposed methodology. A first order low–pass filter is

$$\frac{X_f(s)}{X(s)} = \frac{1}{\tau s + 1} \tag{18}$$

where $X_f(s)$ is the filtered signal, $X(s)$ is the unfiltered signal, τ is the time constant and τ^{-1} is the filter break frequency (rad/s). The break frequency is selected to be 2π to provide a cut off frequency of 1 Hz; therefore, τ = 0.159 s. Transforming equation (18) into the discrete–time domain with a zero order hold and T_s = 0.01 s

$$\frac{X_f(z)}{X(z)} = \frac{6.882 \cdot 10^{-2}}{z - 0.9391} \tag{19}$$

Transforming equation (18) into the discrete–time domain with a zero order hold and T_s = 0.01 s

$$\frac{X_f(z)}{X(z)} = \frac{0.4664}{z - 0.5336} \tag{20}$$

A fourth order Butterworth filter with a 1 Hz cutoff frequency and T_s = 0.01 s is

$$\frac{Xf(z)}{X(z)} = \frac{8.982 \cdot 10^{-7} z^4 + 0.3594 \cdot 10^{-5} z^3 + 0.5391 \cdot 10^{-5} z^2 + 0.3594 \cdot 10^{-5} z + 8.982 \cdot 10^{-7}}{z^4 - 3.836 z^3 + 5.521 z^2 - 3.534 z + 0.8486} \tag{21}$$

A fourth order Butterworth filter with a 1 Hz cutoff frequency and T_s = 0.1 s is

$$\frac{Xf(z)}{X(z)} = \frac{4.826 \cdot 10^{-3} z^4 + 1.935 \cdot 10^{-2} z^3 + 2.891 \cdot 10^{-2} z^2 + 1.937 \cdot 10^{-2} z + 4.827 \cdot 10^{-3}}{z^4 - 2.366 z^3 + 2.314 z^2 - 1.055 z + 0.1874} \tag{22}$$

Plots of filters' performances are shown for the transient portion of the response in Figure 5 for T_s = 0.01 s and in Figure 6 for T_s = 0.1 s. Values of Q = 0.01 and Q = 0.25 are selected for the Kalman filter with T_s = 0.01 and 0.1 s, respectively. Figures 2.5 and 2.6 show that the Kalman filter outperforms the low–pass and Butterworth filters. All three filters underpredict the measurement for both sample periods. The maximum error of the Butterworth filter is approximately 44% for both sample periods while the low–pass and Kalman filters contain comparable maximum errors at approximately 13%. Less error is present in the Kalman filter estimates in both plots through the majority of the transient portion of the response.

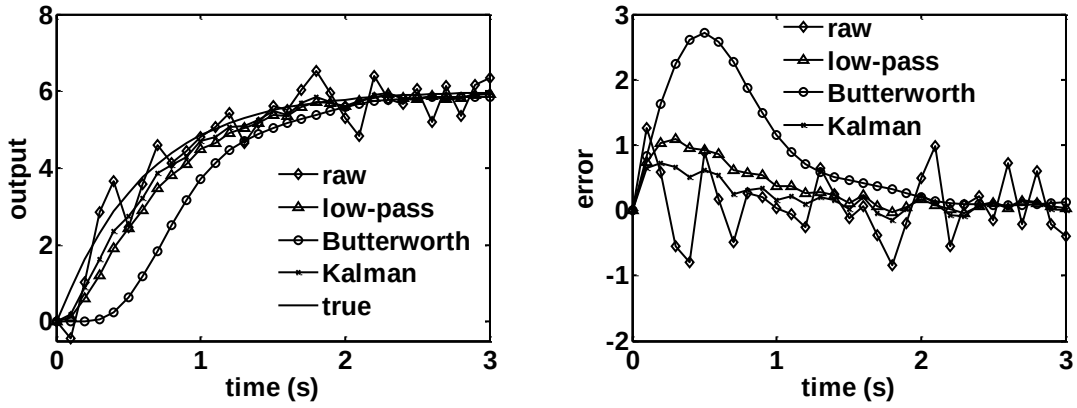

(a) (b)

Figure 5. (a) Output and (b) error for Kalman, low–pass, and Butterworth filters, T_s = 0.01 s.

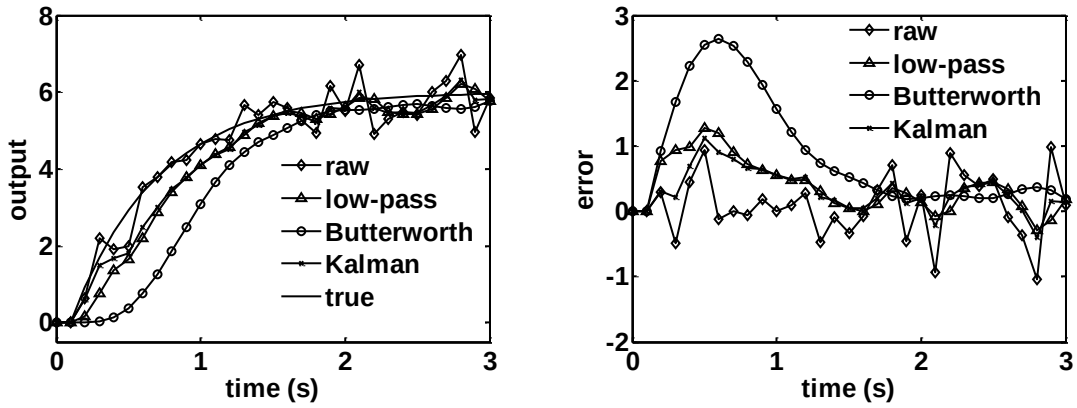

(a) (b)

Figure 6. (a) Output and (b) error for Kalman, low–pass, and Butterworth filters, T_s = 0.1 s.

C. Modeling

The Recursive Least Squares technique (Åström and Wittenmark, 1995) is used to develop system models from the filtered and raw signals. The model responses for a step input are shown in Figs. 7 and 8 for T_s = 0.01 and 0.1 s, respectively. The model coefficients and percent error are shown in Tables 2.1 and 2.2 for T_s = 0.01 and 0.1 s, respectively. The model constructed from the data processed with the Kalman filter is the most accurate in terms of coefficient estimates, transient response, and steady–state error. The model constructed from the data processed with the Butterworth filter has significant errors due to the phase shift created by the Butterworth filter. The model constructed from the raw data contains the most error since the noise distorts the system dynamics.

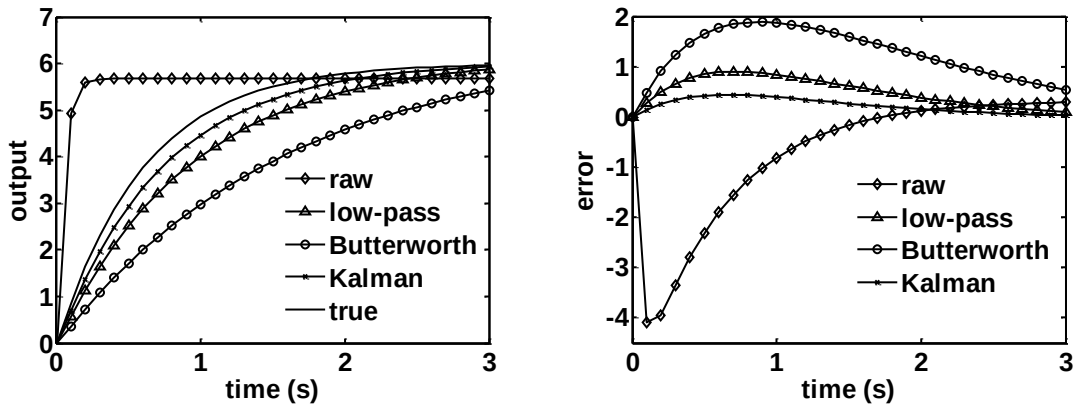

(a) (b)

Figure 7. Model (a) output and (b) error using raw data, low–pass, Butterworth, and Kalman filters, T_s = 0.01 s.

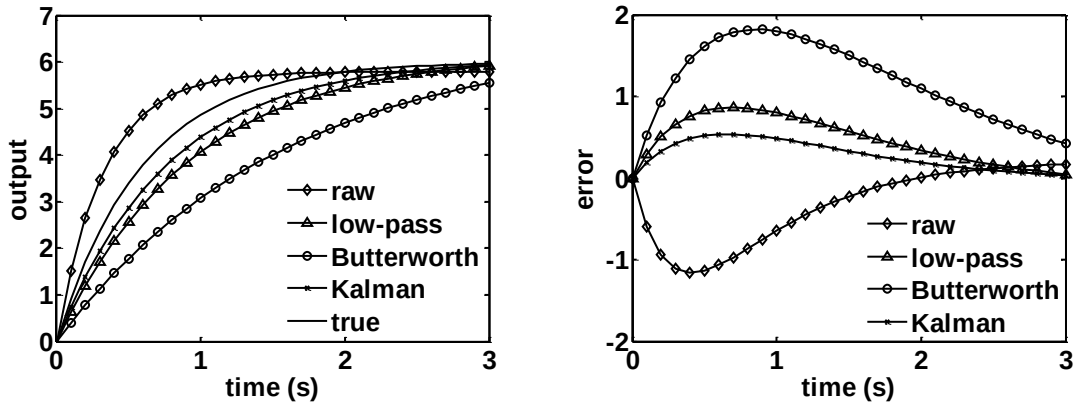

(a) (b)

Figure 8. Model (a) output and (b) error using raw data, low–pass, Butterworth, and Kalman filters, T_s = 0.1 s.

Table 1. Coefficient estimates for models with T_s = 0.01 s, a = –0.983, and b = 0.100.

	a		b	
	estimate	**error (%)**	**estimate**	**error (%)**
raw data	-0.797	19.0	1.15	1060
low-pass	-0.989	0.596	$6.57 \cdot 10^{-2}$	34.1
Butterworth	-0.994	1.04	$4.05 \cdot 10^{-2}$	59.3
Kalman	-0.986	0.315	$8.15 \cdot 10^{-2}$	18.2

Table 2. Coefficient estimates for models with T_s = 0.01 s, a = –0.846, and b = 0.922.

	a		b	
	estimate	**error (%)**	**estimate**	**error (%)**
raw data	-0.737	12.9	1.52	64.8
low-pass	-0.897	6.04	0.631	31.5
Butterworth	-0.938	10.8	0.404	56.2
Kalman	-0.879	3.88	0.732	20.6

The filtering methodology can be used to filter data prior to empirical modeling to acquire a more reliable model. Since this filter relies on model–based estimation, it has always been necessary to have a precise model of the system dynamics to ensure proper

filter performance. However, the stochastic process model provides a way to use a Kalman filter for state estimation with limited knowledge of the system behavior.

III. FRICTION STIR WELDING EXAMPLE

Friction Stir Welding is a new welding technique capable of joining traditionally hard to join materials such as 2000 and 7000 series aluminum alloys (Mishra and Ma, 2005). The process utilizes a rotating, non–consumable tool containing a shoulder and profiled pin to induce gross plastic deformation along a weld path. In a FSW process, the tool is plunged into the material at a specified spindle speed, ω, until the shoulder contacts the material and is then left to dwell for a specified period of time to soften the surrounding area. The tool then advances along its weld path at a traverse rate, v, joining the material as it leaves the processing zone. Schematics of the FSW process are shown in Figure 9.

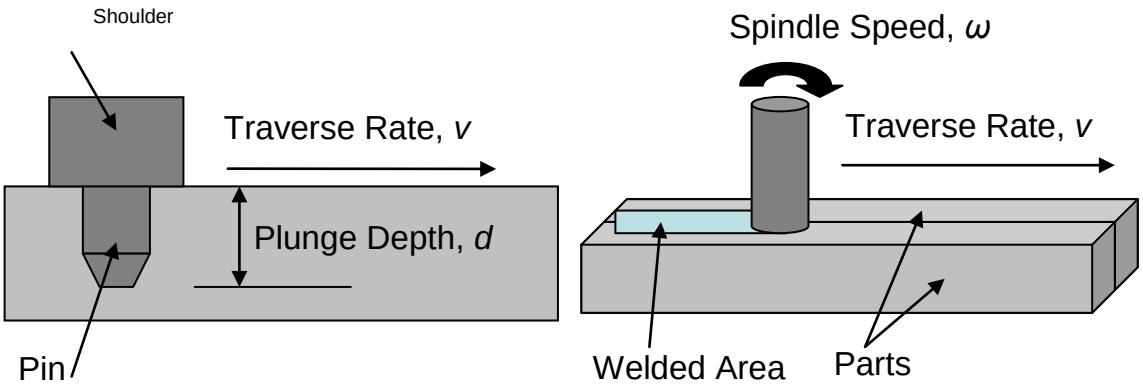

Figure 9: FSW Process Schematics.

Constant process parameter runs in FSW processes can lead to internal defects known as wormholes and surface voids due to improper fixturing of the parts and machine geometric errors. Therefore, the process is typically run in a force control mode in which the traverse rate and spindle speed are held constant while the plunge depth is adjusted on–line to maintain a desired axial force profile. Before a controller can be designed, the system is modeled empirically through a series of step tests. An example of a step test is shown in Figure 10. It can be seen that small changes in plunge depth create large changes in axial force. If no post signal processing is used, the combined process and sensor noise is so large in magnitude that it is difficult to detect changes in the axial force due to changes in the plunge depth. This is particularly apparent between the fourth and fifth step changes. From the experimental data, R = 0.0163 kN^2. The filtering methodology is applied (λ = 0, $Q = 0.05R$ kN^2) to the measurement data in Figure 10, and it is seen that the variance is greatly reduced (i.e., over an order of magnitude) without compromising the phase.

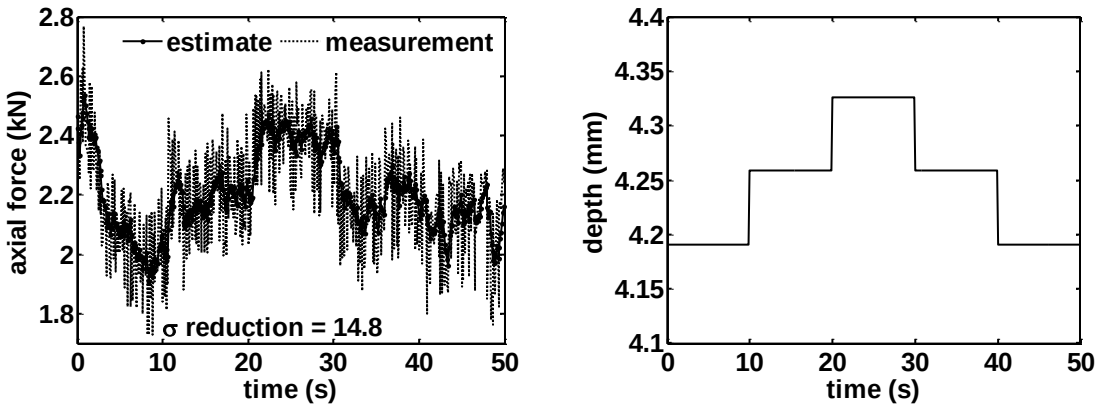

(a) (b)

Figure 10. Step test (a) axial force and (b) plunge depth, v = 2.6 mm/s and ω = 1600 rpm.

A. FSW Process Modeling

Twelve experiments are conducted based on a central composite Design of Experiments (DOE) over the operating range of all three process parameters. The filtering methodology is applied ($\lambda = 0$, $Q = 0.05R$) to all twelve runs. Table 3 shows the process parameters, heat index, and variance reduction ratio for each run. The variance reduction ratio is the unfiltered signal variance divided by the filtered signal variance. The results demonstrate the filtering methodology can reduce signal variance by a factor of 3 to nearly a factor of 17 for FSW processes.

The results from runs 11 and 12 were deemed to be unacceptable and, therefore, were not used to create the dynamic model. This can be explained by the heat index, which is

$$HI = \frac{\omega^2}{10^4 v} \tag{23}$$

Note the traverse rate is given in inches per minute when calculating the heat index. Runs 11 and 12 had particularly low heat indices, although they were not the lowest. A low heat index can lead to a “cold run” that sometimes produces poor welds.

Table 3. Process parameters and variance reduction for FSW runs used for process modeling.

Run	*v* (mm/s)	*ω* (rpm)	*HI* (rpm^2/ipm)	Variance Reduction Ratio
1	2.60	1600	41.7	11.3
2	2.60	1900	58.8	3.11
3	2.18	1810	63.6	4.91
4	3.02	1390	27.1	12.9
5	2.60	1600	41.7	7.08
6	3.02	1810	45.9	8.25
7	2.18	1390	37.5	16.9
8	3.02	1390	27.1	5.22
9	2.18	1810	63.6	3.07
10	2.00	1600	54.2	7.23
11	3.20	1600	33.9	12.1
12	2.60	1300	27.5	6.01

An empirical second order model of the process and equipment dynamics is

$$\frac{F(z)}{U(z)} = v^{\alpha}\omega^{\beta}\,\frac{b_1 z + b_2}{z^2 + a_1 z + a_2}\,z^{-n_d} \tag{24}$$

where $F(z)$ is the axial force, $U(z)$ is the control signal, n_d is the number of delay periods, and b_1, b_2, a_1, a_2, α, and β are model coefficients. The model structure is based upon visual inspection of the runs in Table 3. The control signal and plunge depth are related by

$$u(k) = d^{\gamma}(k) \tag{25}$$

where γ is a model coefficient. The model coefficients α, β, and γ are found by using the steady–state model

$$F_{ss} = Cv^{\alpha}\omega^{\beta}d^{\gamma} \tag{26}$$

where F_{ss} is the average steady–state axial force and C is the steady–state gain. Taking the natural log of both sides of equation (19)

$$\ln(F_{ss}) = \ln(C) + \alpha\ln(v) + \beta\ln(\omega) + \gamma\ln(d) \tag{27}$$

and applying Least Squares to the data in runs 1–10, $C = 6.18 \cdot 10^{-2}$, $\alpha = 0.185$, $\beta = -0.374$, and $\gamma = 2.65$. Transforming equation (24) into the discrete–time domain using a zero order hold

$$F(k) = -a_1 F(k-1) - a_2 F(k-2) + v^{\alpha} \omega^{\beta} \left[b_1 u(k-1-n_d) + b_2 u(k-2-n_d) \right] \quad (28)$$

where n_d is determined to be 5 iterations by visually inspecting the step tests. Recursive Least Squares is used to determine the model coefficients b_1, b_2, a_1, and a_2. A complete covariance reset is employed if any of the diagonals of the covariance matrix become less than ten percent of their initial value. After the algorithm is executed for runs 1–10, the model coefficient sets are averaged and the transfer function is

$$\frac{F(z)}{U(z)} = v^{0.185} \omega^{-0.374} \frac{1.22 \cdot 10^{-2} z}{z^2 - 0.848z + 4.77 \cdot 10^{-2}} z^{-5} \quad (29)$$

The same empirical model is now constructed in the same manner as above using the unfiltered data. In this case the transfer function is

$$\frac{F(z)}{U(z)} = v^{0.189} \omega^{-0.372} \frac{6.04 \cdot 10^{-2} z - 6.2 \cdot 10^{-3}}{z^2 - 7.34 \cdot 10^{-2} z - 3.48 \cdot 10^{-2}} z^{-5} \quad (30)$$

The response of each model is now compared to the measured data. An example is shown in Figure 11. Both dynamic models predict steady–state values within five percent of each other. The model in equation (29) contains two overdamped poles with time constants of $3.57 \cdot 10^{-2}$ s and 0.418 s. The model in equation (30) contains two overdamped poles with time constants of $6.74 \cdot 10^{-2}$ s and $5.33 \cdot 10^{-2}$ s. Based on the work of Zhao et al. (2007), the system is dominated by a time constant of 0.519 s. This implies the model acquired through the use of the unfiltered data is not reliable and should not be used for controller design.

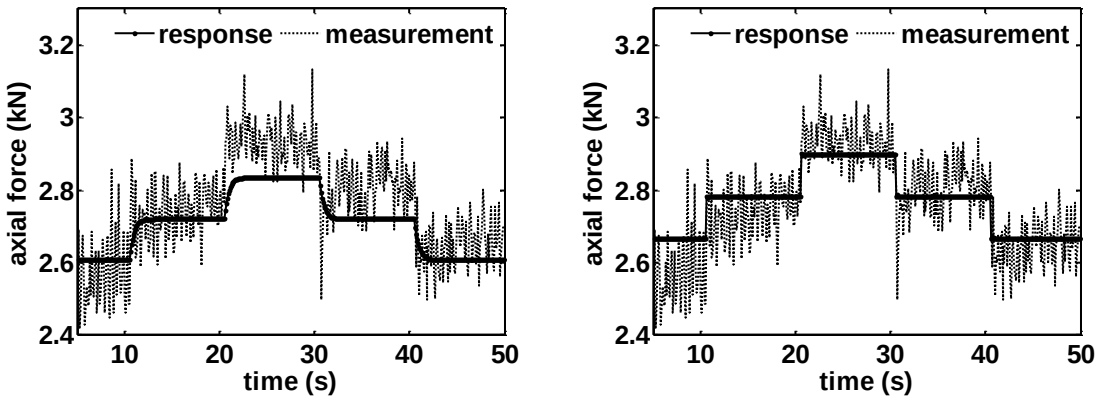

(a) (b)

Figure 11. Measured response compared to (a) response of model developed using filtered data and (b) response of model developed using raw data, v = 3.02 mm/s, ω = 1810 rpm, and plunge depth profile in Figure 10b.

B. FSW Process Control

A general tracking controller with constant disturbance rejection is designed to control the axial force. The block diagram is shown in Figure 12. The transfer function is

$$G(z) = \frac{b(z)}{a(z)} \tag{31}$$

The disturbance generating polynomial is

$$v(z) = z - 1 \tag{32}$$

The controller polynomial is

$$g(z) = g_1 z^2 + g_2 z + g_3 \tag{33}$$

where g_1, g_2, and g_3 are chosen to shape the closed–loop system error dynamics. The closed error dynamics are third order with one overdamped pole and two underdamped poles. The time constant of the overdamped pole is τ_1 = 0.03 s and the two underdamped

poles are characterized by a natural frequency of 10 and a damping ratio of 0.5. Equating the actual and desired closed–loop characteristic polynomials

$$v(z)a(z)-g(z)=z^3-0.8216z^2+0.3959z-1.311\cdot10^{-2} \tag{34}$$

Equation like coefficients in z in equation (34), g_1 = –1.026, g_2 = 0.4994, and g_3 = –0.3460. The control signal is

$$\begin{aligned} u(k)=&\frac{1}{b_1}\left[F_r(k+1)+(a_1-1)F_r(k)+(a_2-a_1)F_r(k-1)-a_2F_r(k-2)\right]\\ &-\frac{1}{b_1}\left[g_1E_1(k)-g_2E_1(k-1)-g_3E_1(k-2)\right]\\ &+\frac{1}{b_1}\left[(b_2-b_1)u(k-1)+b_2u(k-2)\right] \end{aligned} \tag{35}$$

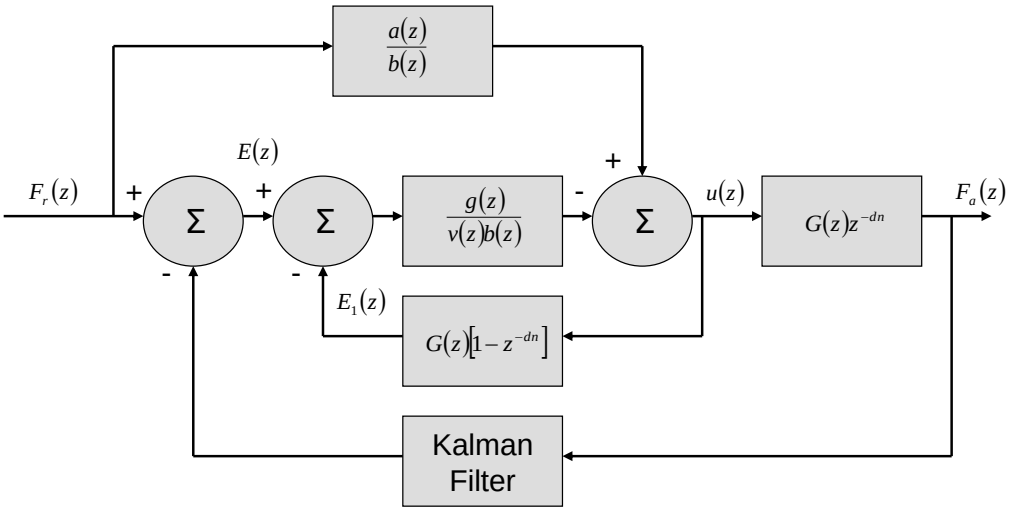

Figure 12. Axial force closed–loop system block diagram.

The controller is implemented on the FSW platform with saturation limits on the plunge depth set between 4.17 mm and 4.8 mm to ensure the shoulder does not lose contact with the material surface. The imposed rate limitation on change in plunge depth is 0.5 mm/s to prevent tool breakage.

In the first experiment the axial force controller uses the unfiltered measurement to track $F_r(t)$ = 2.7 kN. The traverse rate and spindle speed are 2.18 mm/s and 1810 rpm, respectively. The results are plotted in Figure 13. The controller maintains a constant force with an average 2.74 kN and standard deviation of 0.1910 kN; however, the average absolute error during the steady–state portion is 0.3410 kN and large axial force oscillations occur due to the large amounts of variation present in the raw measurement signal. The plunge depth continuously oscillates between its saturation limits.

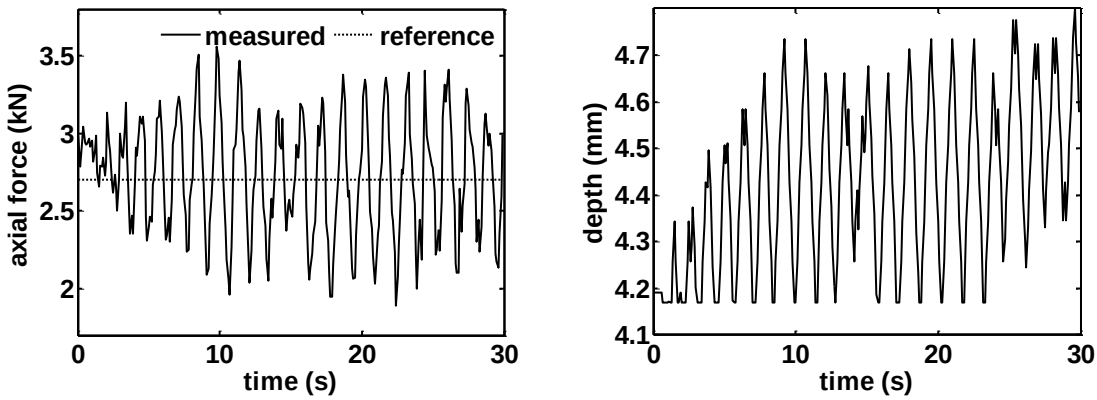

(a) (b)

Figure 13. Axial force controller results using unfiltered measurement and $F_r(t)$ = 2.7 kN, (a) axial force and (b) plunge depth.

In the second experiment the axial force controller uses the filtered measurement to track $F_r(t)$ = 2.7 kN. The traverse rate and spindle speed are 2.18 mm/s and 1810 rpm, respectively. The results are shown in Figure 14. In this case the average axial force is 2.705 kN, standard deviation of $4 \cdot 10^{-4}$ kN, and absolute average error of 0.1064 kN during the steady–state portion. The filter effectively reduces the magnitude of the

oscillations in both the axial force and plunge depth. Implementation of the filtering methodology allows for a wider range of reference tracking as the controller is no longer continuously saturating.

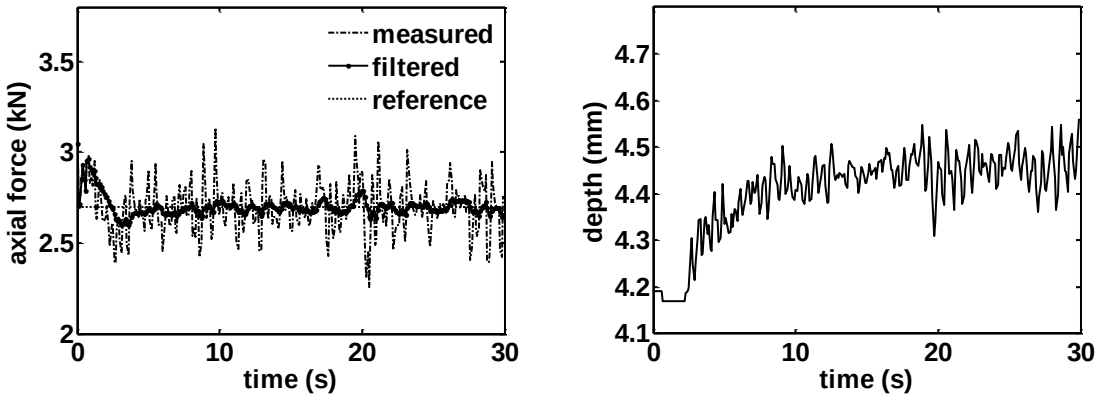

(a) (b)

Figure 14. Axial force controller results using filtered measurement and $F_r(t)$ = 2.7 kN, (a) axial force and (b) plunge depth.

Next, the axial force controller is used to track a time varying reference of

$$F_r(t) = 2.7 + 0.1Sin(0.8\pi t) \tag{36}$$

In the third experiment the axial force controller uses the unfiltered measurement to track the reference signal in equation (36). The traverse rate and spindle speed are 2.18 mm/s and 1810 rpm, respectively. The results are shown in Figure 15. As in Figure 13, the controller is able to adequately track the desired reference, but with considerable oscillations and continuous plunge depth saturation. For this experiment the average absolute error is 0.4131 kN during the steady–state portion of the response.

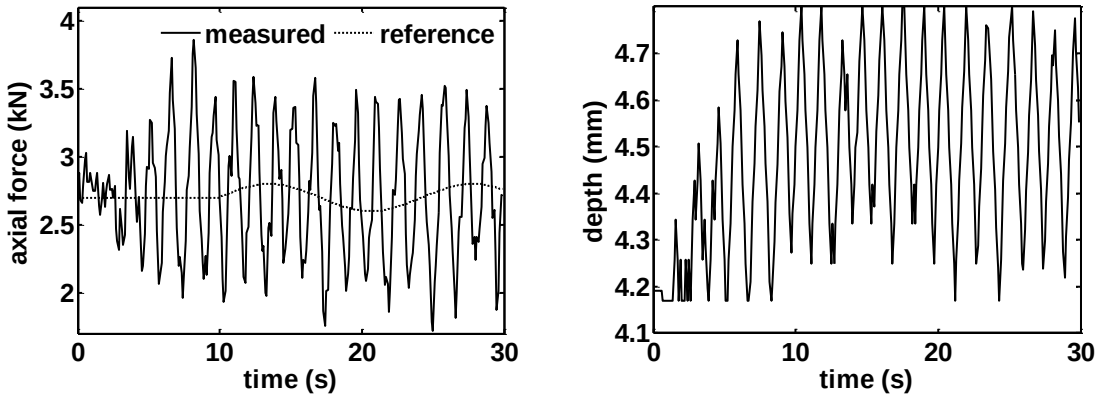

(a) (b)

Figure 15. Axial force controller results using unfiltered measurement and reference force in equation (36), (a) axial force and (b) plunge depth.

In the fourth experiment the axial force controller uses the filtered measurement to track the reference signal in equation (36). The traverse rate and spindle speed are 2.18 mm/s and 1810 rpm, respectively. The results are shown in Figure 16. Similar to Figure 14, the filter effectively reduces the magnitude of the axial force oscillations and allows for a wider range of reference signals to be utilized since the plunge depth is not saturating during the steady–state response. For this experiment the average absolute error is 0.1242 kN during the steady–state portion of the response.

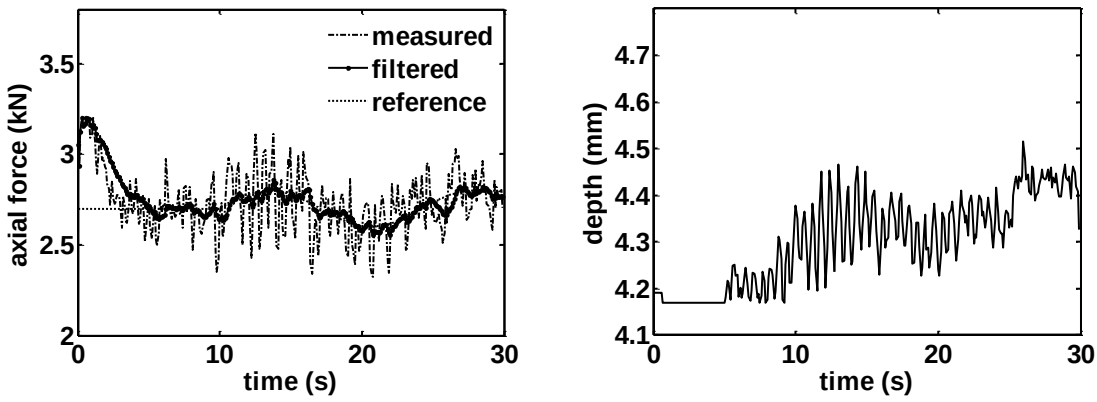

(a) (b)

Figure 16. Axial force controller results using filtered measurement and reference force in equation (36), (a) axial force and (b) plunge depth.

IV. LASER METAL DEPOSITION EXAMPLE

Laser Metal Deposition is an important Solid Freeform Fabrication technique that allows direct fabrication of functional metal parts directly from CAD solid models (Liou et al., 2007). The process can also be used for part repair, thereby extending product service life. Generally a LMD system consists of a multiple–axis motion system, a laser, and a powder feeder (Figure 17). During the process, a powder stream is injected into a laser generated melt pool on the substrate. With the axis moving, the melt pool quickly solidifies and forms a clad; thus, the injected powder is metallurgically bonded with the substrate. Depending on the trajectory of the motion system, parts with complex geometries can be fabricated in a layer–by–layer manner. Melt pool temperature control is an important control problem in LMD because it affects the part microstructure, which is highly related to the material properties. The measurement signal has tremendous variations that may deteriorate the controller performance. The application of the filtering

methodology to the temperature measurement signal will significantly reduce measurement signal variation, resulting in improved controller performance.

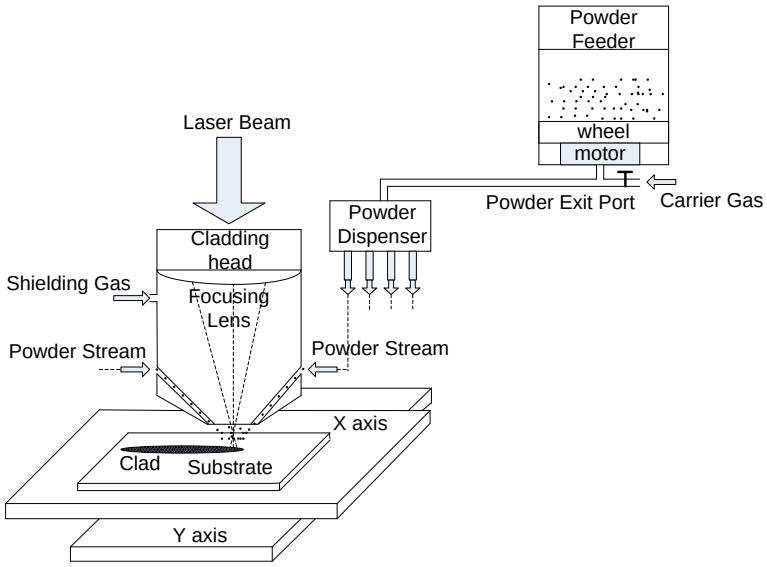

Figure 17. LMD system schematic.

To illustrate the affect the filtering methodology has on the measured temperature signal, an open–loop test is conducted. In this experiment the powder flow rate is 4 g/min and the traverse speed is 4 ipm. The powder material is H13 tool steel with particles having a mean diameter of 100 μm. The filtered and measured temperature signals are shown in Figure 18. It can be observed that with the Kalman filter, the magnitude of the variation becomes smaller.

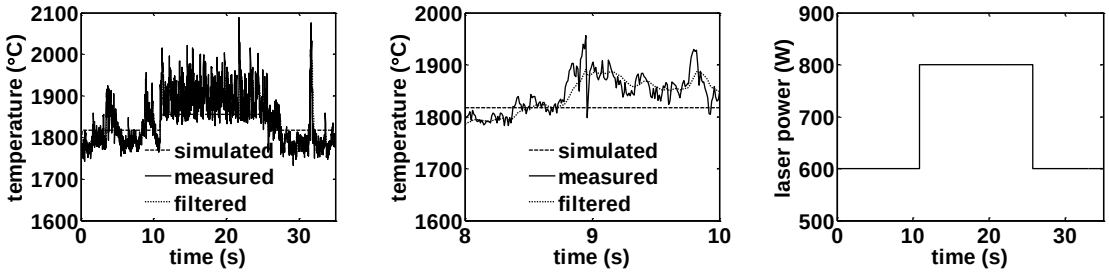

(a) (b) (c)

Figure 18. Open–loop LMD test with T_s = 0.01 s, λ = 0, R = 2500, Q = 25, (a) temperature versus time, (b) zoomed–in view of temperature versus time, and (c) laser power versus time.

A. LMD Process Modeling

The melt pool temperature is modeled using the following model

$$T(s) = \frac{K}{\tau s + 1} V^{\alpha}(s) Q^{\beta}(s) M^{\gamma}(s) \tag{37}$$

where T is the melt pool temperature (°C), V is the traverse speed (ipm), Q is the laser power (W), M is the powder flow rate (g/min), K is the system gain, and τ is the time constant (s). Transforming equation (35) into the discrete–time domain using a zero order hold

$$T(z) = \frac{b_0}{z + a_0} V^{\alpha}(z) Q^{\beta}(z) M^{\gamma}(z) \tag{38}$$

where $a_0 = -e^{-T_s/\tau}$ and $b_0 = K\left(1 - e^{-T_s/\tau}\right)$. To determine the model coefficients K, α, β, and γ, the steady–state portion of equation (38) is considered

$$T_{ss} = K v^{\alpha} q^{\beta} m^{\gamma} \tag{39}$$

where T_{ss} is the average steady–state temperature. A series of experiments, covering the process operating range, are designed using DOE. The results are listed in Table 4. The

parameters are estimated using the Least Squares method based on the data listed in Table 4 and are found to be $K = 1170$, $\alpha = -8.18 \cdot 10^{-3}$, $\beta = 7.16 \cdot 10^{-2}$, and $\gamma = 3.42 \cdot 10^{-3}$.

Table 4. Experimental results for model coefficient identification of LMD process.

Run	*Q* (W)	*m* (g/min)	*v* (ipm)	ave(*T*) (ºC)
1	600	4	8	1851
2	700	4	4	1861
3	800	6	4	1911
4	600	6	6	1835
5	700	8	6	1854
6	800	4	6	1854
7	600	8	4	1842
8	700	6	8	1857
9	800	8	8	1881

To determine the time constant, an experiment where the laser power is increased and decreased in a step–wise manner is conducted. For this experiment, $m = 4$ g/min and $v = 4$ ipm. The measured temperature data is filtered using the filtering methodology with $\lambda = 0$, $R = 2500$, and $Q = 25$. Recursive Least Squares is then applied to estimate the time constant. The value of the time constant is determined to be $\tau = 7.27 \cdot 10^{-2}$ s. The model response is compared to the filtered measurement data in Figure 18.

B. LMD Process Control

Letting $U(z) = V^{\alpha}(z)Q^{\beta}(z)M^{\gamma}(z)$, equation (38) becomes

$$T(z) = \frac{b_0}{z + a_0} U(z) \tag{40}$$

A general tracking controller using the Internal Model Principle is designed to regulate the melt pool temperature. The block diagram is shown in Figure 19.

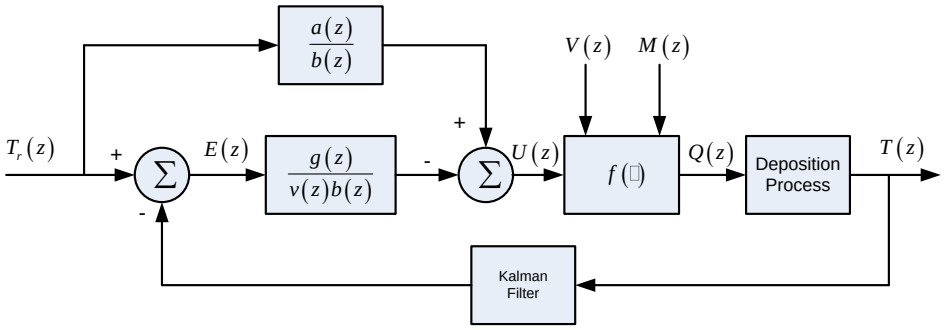

Figure 19. Melt pool temperature closed–loop control system block diagram.

With the disturbance generating polynomial given by equation (32) and a closed–loop characteristic polynomial $v(z)a(z)–g(z)$ with two poles at $-e^{-T_s/\tau_1}$ and $-e^{-T_s/\tau_2}$, where τ_1 = 0.1 s and τ_2 = 0.11 s, the controller polynomial is

$$g(z) = g_1 z + g_0 = \left(e^{-T_s/\tau_1} + e^{-T_s/\tau_2} - 1 - e^{-T_s/\tau}\right)z + \left(e^{-T_s/\tau} - e^{-T_s/\tau_1 - T_s/\tau_2}\right) \tag{41}$$

The control signal is

$$u(k) = u(k-1) + \frac{T_r(k+1) - \left(1 + e^{-T_s/\tau}\right)T_r(k) + e^{-T_s/\tau}T_r(k-1) - g_1 e(k) - g_0 e(k-1)}{K\left(1 - e^{-T_s/\tau}\right)} \tag{42}$$

and the commanded laser power is

$$q(k) = \left(\frac{u(k)}{v(k)^{\alpha}\, m(k)^{r}}\right)^{1/\beta} \tag{43}$$

In the first experiment the temperature controller uses the unfiltered measurement to track $T_r(t)$ = 1900 °C. The mass flow rate and traverse rate are 6 g/min and 6 ipm, respectively. The results are shown in Figure 20. For this experiment, the average melt pool temperature is 1904 °C, the average absolute error is 61.8 °C, and error standard

deviation is 76.8 °C. The results show that significant variation exists in both the temperature and the laser power signals.

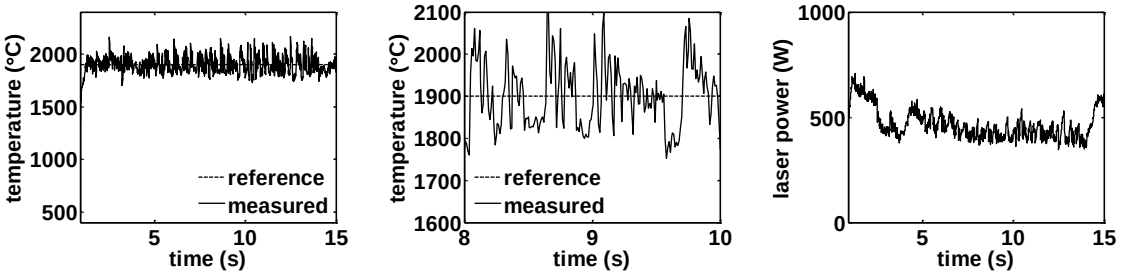

(a) (b) (c)

Figure 20. Temperature controller results using unfiltered measurement and $T_r(t)$ = 1900 °C, (a) temperature versus time, (b) zoomed–in view of temperature versus time, and (c) laser power versus time.

In the second experiment the temperature controller uses the filtered measurement to track $T_r(t)$ = 1900 °C. The mass flow rate and traverse rate are 6 g/min and 6 ipm, respectively. The results are shown in Figure 21. For this experiment, the average melt pool temperature is 1901 °C, the average absolute error is 42.3 °C, and error standard deviation is 57.9 °C. The results show that the average absolute error is reduced by 31.6% and the error standard deviation is reduced by 24.6%.

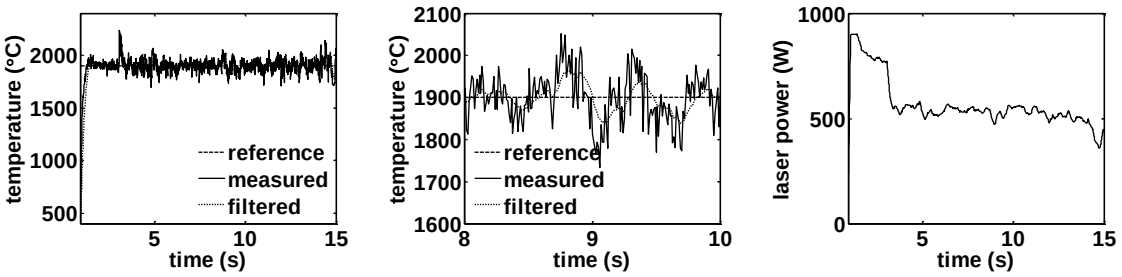

(a) (b) (c)

Figure 21. Temperature controller results using filtered measurement and $T_r(t)$ = 1900 °C, (a) temperature versus time, (b) zoomed–in view of temperature versus time, and (c) laser power versus time.

The performances of the controllers are now compared when tracking a time varying reference. The temperature reference for these experiments is

$$T_r(t) = 1850 + 50\sin(t) \tag{44}$$

In the third experiment the temperature controller uses the unfiltered measurement to track the temperature reference given in equation (44). The mass flow rate and traverse rate are 6 g/min and 6 ipm, respectively. The results are shown in Figure 22. The average absolute error is 52.9 °C and error standard deviation is 71.0 °C. The results show that significant variation exists in both the temperature and the laser power signals due to the fact that the controller operates on the unfiltered signal.

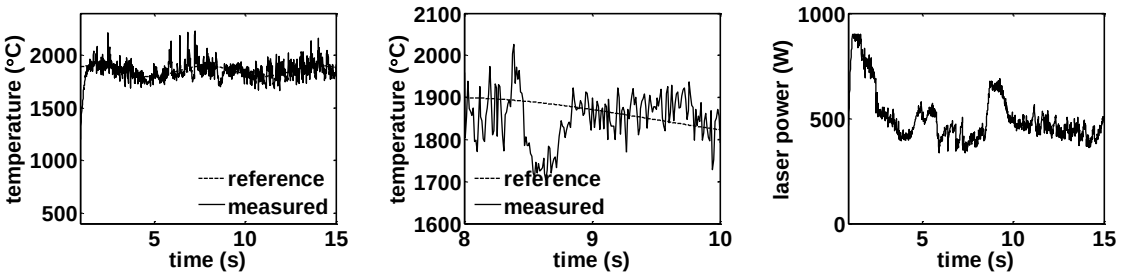

(a) (b) (c)

Figure 22. Temperature controller results using unfiltered measurement and reference temperature given in equation (44), (a) temperature versus time, (b) zoomed–in view of temperature versus time, and (c) laser power versus time.

In the third experiment the temperature controller uses the filtered measurement to track the temperature reference given in equation (44). The mass flow rate and traverse rate are 6 g/min and 6 ipm, respectively. The results are shown in Figure 23. The average absolute error is 40.8 °C and error standard deviation is 55.7 °C. Compared with the results in Figure 22, the average absolute error is reduced by 22.9% and error standard deviation is reduced by 21.6%. Also, the oscillations in the temperature and laser power signals have been greatly reduced.

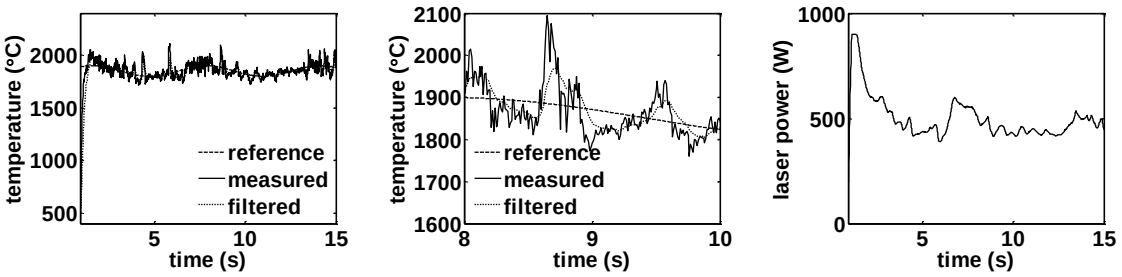

(a) (b) (c)

Figure 23. Temperature controller results using filtered measurement and reference temperature given in equation (44), (a) temperature versus time, (b) zoomed–in view of temperature versus time, and (c) laser power versus time.

V. SUMMARY AND CONCLUSIONS

The filtering methodology is applied to control of the axial force in a Friction Stir Welding process. Two sets of experiments are performed to test constant and time varying references under filtered and unfiltered conditions. Results show that the Kalman filtering methodology improves controller performance and allows for a wider variety of inputs without saturating the control signal.

The Kalman filter introduced in the above context has been applied to the melt pool temperature control in the laser metal deposition process. Two experiments, regarding the tracking of two different references: constant and time varying, are conducted. The experimental results show that the application of the Kalman filter in the melt pool temperature control helps to improve the controller performance by reducing the tracking error and melt pool temperature variations.

VI. REFERENCES

Åström, K.J. and Wittenmark, B., 1995, Adaptive Control, Addison–Wesley, New York.

Bhattacharyya, P. and Sengupta, D., 2007, "Estimation of Tool Wear Based on Adaptive Sensor Fusion of Force and Power in Face Milling," *International Journal of Production Research,* Vol. 43, pp. 1 – 17.

Freitag, K.P., 2004, "Two–Axis Force Feedback Deflection Compensation of Miniature Ball End Mills," Mechanical Engineering Department, North Carolina State University (NCSU).

Ghosh, N., Ravi, Y.B., Patra, A., Mukhopadhyay, S., Paul, S., Mohanty, A.R., and Chattopadhyay, A.B., 2007, "Estimation of Tool Wear during CNC Milling Using Neural Network Based Sensor Fusion," *Mechanical Systems and Signal Processing*, Vol. 21, pp. 466–479.

Liang, M., Yeap, T., Rahmati, S., and Han, Z., 2002, "Fuzzy Control of Spindle Power in End Milling Processes," *International Journal of Machine Tools and Manufacture*, Vol. 42, pp. 1487–1496.

Liou, F.W., Slattery, K., Kinsella, M., Newkirk, J., Chou, J–N., and Landers, R.G., 2007, "Applications of a Hybrid Manufacturing Process for Fabrication of Metallic Structures," *Journal of Rapid Prototyping*, Vol. 13, No. 4, pp. 236–244.

Mishra, R.S. and Ma, Z.Y., 2005, "Friction Stir Welding and Processing," *Materials Science and Engineering: R*, Vol. 50, No. 1–2, pp. 1–78.

2. DESIGN AND IMPLEMENTATION OF A GENERAL TRACKING CONTROLLER FOR FRICTION STIR WELDING PROCESSES

Oakes, T., Landers, R. G.
Department of Mechanical and Aerospace Engineering
Missouri University of Science and Technology – Rolla, Missouri, U.S.A 65401
Email: tmo6w3@mst.edu, ltx8d@mst.edu, landersr@mst.edu, bala@mst.edu

ABSTRACT

This paper establishes a method for force filtering, develops a dynamic process model, and designs and implements a general tracking controller to regulate the axial force for a variety of reference signals in Friction Stir Welding processes. Steady state and dynamic models are used to relate the input process parameters to the axial force. The general tracking controller is implemented in a Smith Predictor–Corrector Structure to compensate for a pure communication delay. The controller successfully performs bead–on–plate welds using a 6061 aluminum alloy. Both constant and sinusoidal reference forces are tracked.

I. INTRODUCTION

Friction Stir Welding (FSW) is a solid state joining process that utilizes gross plastic deformation rather than a conventional welding flame to join material. The FSW process is unique in that it can be used to successfully join materials such as aluminum alloys that are difficult to join with other welding processes.

The FSW joining process requires a non–consumable tool, containing a shoulder and profiled pin region. The tool is plunged into the part at a specified spindle speed and plunge rate until the shoulder makes contact with the material to be joined. Following a

brief dwell period, the rotating tool advances along the weld path at a specified traverse rate and spindle rotation speed. The combination of heat input and tool geometry cause the material along the boundaries of the weld region to deform and mix together to form a solid joint. A process schematic is shown in Figure 1.

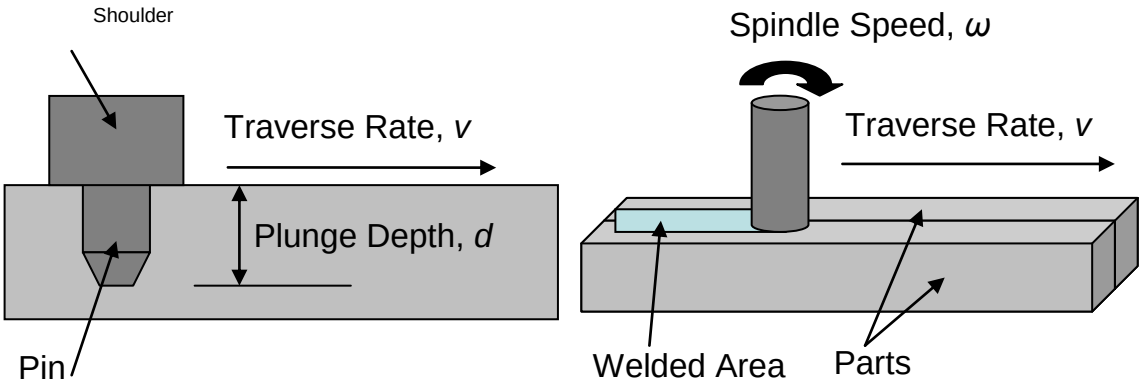

Figure 1. Friction Stir Welding Schematic.

Three common process parameters for the FSW process are traverse rate, v, spindle speed, ω, and plunge depth, d. Constant process parameter runs can result in poor quality welds due to improper fixturing of the work piece, machine geometric errors, and material inconsistencies (i.e., part slope) along the weld path. Cederqvist et al. [2008] fixed values of traverse rate and plunge depth and adjusted the spindle speed online with a Proportional plus Integral plus Derivative controller to regulate the tool pin temperature. The method is effective, but the closed–loop response is sluggish due to the inherent low bandwidth of thermal systems. Zhao et al. [2007] conducted a FSW process with constant traverse rate and spindle speed while varying the plunge depth to control the axial force. A polynomial pole placement technique was used to design a controller

based on a desired characteristic equation. The controller was designed specifically to reject constant disturbances and allow tracking of constant axial forces. Kalya [2007] regulated the axial force in a similar manner using an adaptive neural network controller to account for variations in the model dynamics. The axial force is regulated in this paper to ensure the tool maintains proper contact with the part to avoid creating excessive flash and defects such as surface voids and wormholes.

II. EXPERIMENTAL SYSTEM AND FILTERING

An ABB IRB 940 Tricept Robot is retrofitted with a FSW spindle head to provide the desired rotational motion. The spindle is driven by a SLM115–368 servo motor and is rated at 10 hp with a range of ±3000 rpm. A six axis force/moment sensor (JR3 Inc. model 75E20S–M125A–A 6000N1150) is used to record the lateral, normal and axial forces, as well as the respective moments. The physical setup is shown in Figure 2.

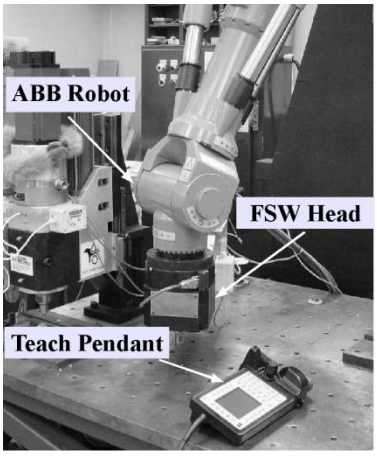

Figure 2. ABB IRB 940 Tricept Robot with FSW Head.

The robot control unit is programmed through RAPID, which allows the operator to pre program the system motion and control algorithms. The code is typed in text format and uploaded to the control unit. Code is typically divided into subsections including: low–level formatting, primary welding loop, interrupt subroutines, and data collection. A teach pendant is used to load the file, select a welding vector and execute the code.

Tool eccentricity and sensor noise contribute to a large variance in the measured force signals; therefore, a first order stochastic process model is used in conjunction with a two–step Kalman filter to effectively reduce the axial force signal variance while preserving the phase and magnitude. The stochastic process model is

$$f\left(k\right)=e^{-\lambda T}f\left(k-1\right)+w\left(k\right) \tag{45}$$

where f is the axial force, k is the current iteration, T is the sample period, w is the process noise, and λ is a filter tuning parameter. Previous studies have found that $\lambda = 0$ provides the best filtering capability in terms of steady–state behavior. The process measurement is

$$y\left(k\right)=F\left(k\right)+v\left(k\right) \tag{46}$$

where F is the measured axial force and v is the measurement noise. The process and measurement noise characteristics, respectively, are

$$w\sim N\left(0,Q\right) \qquad E\left[\left(w\left(k\right)\right)\left(w\left(k\right)\right)^{T}\right]=Q \tag{47}$$

$$v\sim N\left(0,R\right) \qquad E\left[\left(v\left(k\right)\right)\left(v\left(k\right)\right)^{T}\right]=R \tag{48}$$

where R is the measurement variance determined by analyzing steady–state data and is

$$R = \frac{1}{N-1}\sum_{i=1}^{N}\left[\left(y_i - \bar{y}\right)^2\right] \tag{49}$$

where y_i is the steady–state force measurement at the i^{th} iteration, $\bar{y}$ is the measurement average, and N is the number of data points. The parameter Q is the model variance and is adjusted with respect to R to tune the filter. Experimentally, a value of $Q = 0.05R$ is selected for this filter. The filter effectively reduces the signal variance by an order of magnitude while preserving the phase and magnitude.

III. DYNAMIC MODELING

A series of step tests are conducted to obtain a relationship between axial force and commanded plunge depth for use in designing the axial force controller. The tests are conducted using a 6061–T6 aluminum alloy with material composition: 97.9% Al, 0.60% Si, 0.30% Cu, 1.0% Mg, and 0.20% Cr. The tool is tapered, threaded, and contains three flats. The FSW bead–on–plate method is conducted during the testing with a single solid 6.35 mm thick plate. This method does not involve the actual joining of parts; rather, the pin processes solid material. Bead–on–plate welding is commonly used in initial testing to analyze the process without disturbances generated by gaps between the parts. The input process parameters are selected as the plunge depth, traverse rate, and spindle rotation speed. Other factors, such as travel angle and work angle, are held as constant during all runs and, therefore, are not included in the modeling. During each run the transverse rate and spindle speed remain constant, while the plunge depth varies between 4.191–4.716 mm. Note that the shoulder contacts the part at a plunge depth of 4.17 mm. Based on empirical observations, the minimum and maximum traverse rates are 2.0 and 3.2 mm/s, respectively, and the minimum and maximum spindle rotation speeds are 1300

and 1900 rpm, respectively. The selected test conditions are based on a Central Composite Design of Experiments (DOE) and are shown in Table 1.

Table 1. Process Parameters for Step Testing of Plunge Depth.

RUN	Traverse Rate, v (mm/s)	Rotational Speed, ω (rpm)	Heat Index (rpm^2/ipm
1	2.6	1600	98.5
2	2.6	1900	138.8
3	2.18	1810	150.3
4	3.02	1390	64.0
5	2.6	1600	98.5
6	3.02	1810	108.5
7	2.18	1390	88.6
8	3.02	1390	64.0
9	2.18	1810	150.3
10	2	1600	128.0
11	3.2	1600	80.0
12	2.6	1300	65.0

Measured axial force and plunge depth data, as well as commanded plunge depth data, are obtained for each run at a sample rate of 10 Hz. Results from runs 11 and 12 had poor signal to noise ratios and, thus, were excluded from system modeling. This resulted from the runs being very cold, as shown by their low values of heat index in Table 1. An example of the collected force data is shown in Figure 3.

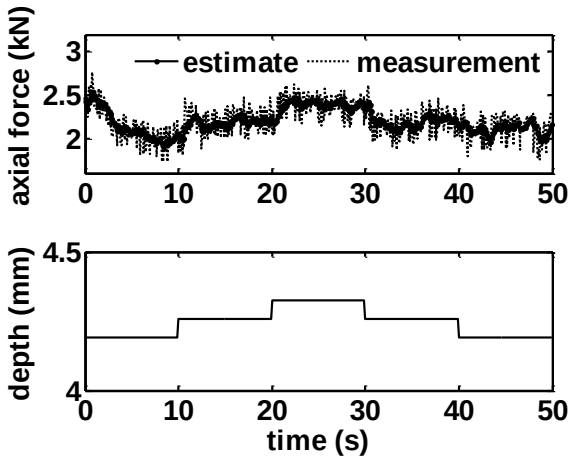

Figure 3. Step Test Force Results and Filter Estimates for Run 1 with v = 2.6 mm/s and ω = 1600 rpm.

The data indicates a positive correlation between measured axial force and commanded plunge depth. As the commanded plunge depth increases, the axial force increases and eventually reaches a steady value. The initial drop in the measured axial force signal represents an extra transient portion of the process present only in the beginning of the weld. This portion of the data is ignored in modeling to minimize error. Note the first and fifth segments, as well as the second and fourth segments, of measured axial force occur at the same depth but do not have the same average force. This is due to machine geometric errors and stiffness, as well as the amount of flash that is generated. As the amount of flash increases, the depth–force relationship is affected due to less material being present in the weld path to resist the tool.

A static power model that relates the steady–state axial force to the input process parameters is

$$F_a = Cv^{\alpha}\omega^{\beta}d^{\gamma} \tag{50}$$

where C, α, β, and γ are model coefficients. Taking the natural log of both sides of equation (50)

$$\ln\left(F_a\right)=\ln\left(C\right)+\alpha\ln\left(v\right)+\beta\ln\left(\omega\right)+\gamma\ln\left(d\right) \tag{51}$$

Using the Least Squares method the model parameters are determined to be $C = 6.18\cdot10^{-2}$, $\alpha = 0.185$, $\beta = -0.374$, and $\gamma = 2.650$.

An empirical second order model of the process and equipment dynamics is

$$\frac{F_a\left(z\right)}{U\left(z\right)}=v^{\alpha}\omega^{\beta}\,\frac{b_1z+b_2}{z^2+a_1z+a_2}\,z^{-n_d} \tag{52}$$

where $F_a(z)$ is the axial force, $U(z)$ is the control signal, n_d is the number of delay periods, and b_2, b_1, a_2, and a_1 are model coefficients. The delay is due to an inherent communication delay between the processor implementing the force controller that determines the reference plunge depth and the processor that regulates the plunge position. The control signal and plunge depth are related by

$$u\left(z\right)=d^{\gamma}\left(z\right) \tag{53}$$

Equation (52) is transformed into a difference equation and solved for $F_a(k)$

$$\begin{aligned}F_a\left(k\right)=&-a_1F_a\left(k-1\right)-a_2F_a\left(k-2\right)\\&+v^{\alpha}\omega^{\beta}\left[b_1u\left(k-1-n_d\right)+b_2u\left(k-2-n_d\right)\right]\end{aligned} \tag{54}$$

A Recursive Least Squares (RLS) algorithm is used to solve for the unknown coefficients of equation (54). The collection of known system inputs and measured system outputs is

$$\begin{aligned}\boldsymbol{\varphi}\left(k\right)=\big[&-f\left(k-1\right)\quad -f\left(k-2\right)\\&u\left(k-1-n_d\right)\quad u\left(k-2-n_d\right)\big]^T\end{aligned} \tag{55}$$

where $f(k)$ is the filtered force measurement at iteration k. The parameter estimates are

$$\boldsymbol{\eta}=\begin{bmatrix}a_1 & a_2 & b_1 & b_2\end{bmatrix}^T \tag{56}$$

where the initial values are selected to be unity. The gain matrix is

$$\mathbf{q}(k) = \mathbf{P}(k-1)\boldsymbol{\varphi}(k)\left[1+\boldsymbol{\varphi}^T(k)\mathbf{P}(k-1)\boldsymbol{\varphi}(k)\right]^{-1} \tag{57}$$

The parameter estimates are

$$\boldsymbol{\eta}(k) = \boldsymbol{\eta}(k-1)+\mathbf{q}(k)\left[y(k)-\boldsymbol{\varphi}^T(k)\boldsymbol{\eta}(k-1)\right] \tag{58}$$

The matrix covariance is

$$\mathbf{P}(k) = \left[\mathbf{I}-\mathbf{q}(k)\boldsymbol{\varphi}^T(k)\right]\mathbf{P}(k-1) \tag{59}$$

where the diagonals of the initial covariance matrix are all set to 100. If any of the diagonals of the covariance matrix fall below ten percent of their initial value, a covariance reset is employed to ensure that the covariance matrix does not wind down. The number of delay periods is determined to be $n_d = 5$. This number is determined based on the average delay observed in the data sets.

The RLS algorithm is applied to runs 1–10 and the values of the coefficients for each model are determined. These ten sets of coefficients are then averaged to determine the overall system model, as shown in Table 2. The system model is

$$\frac{F_a(z)}{U(z)} = \frac{0.0122z}{z^2-0.8476z+0.0477}z^{-5} \tag{60}$$

The open loop transfer function contains two real roots located at 0.787 and $6.06\cdot10^{-2}$, corresponding to time constants of 0.418 and $3.57\cdot10^{-2}$ s, respectively. There is a zero at $z = 0$. The system is stable and exhibits an overdamped response dominated by the slower time constant. The steady–state gain of equation (16) is $6.10\cdot10^{-2}$, which is 1.29% less than the value of C.

Table 2. Dynamic Model Coefficients.

Run	a_1	a_2	b_1	b_2
1	-7.42E-01	-9.33E-02	-1.31E-02	2.36E-02
2	-1.46E+00	5.61E-01	-1.99E-04	6.63E-03
3	-1.05E+00	2.37E-01	6.73E-03	5.24E-03
4	-8.70E-01	1.15E-01	2.56E-02	-1.04E-02
5	-5.91E-01	-2.25E-01	2.49E-02	-1.43E-02
6	-8.32E-01	5.23E-02	7.66E-03	5.59E-03
7	-7.20E-01	-1.52E-03	1.97E-02	-2.64E-03
8	-7.33E-01	-4.27E-02	2.19E-02	-8.07E-03
9	-9.87E-01	1.48E-01	1.63E-02	-7.24E-03
10	-4.94E-01	-2.74E-01	1.26E-02	1.41E-03
11	n/a	n/a	n/a	n/a
12	n/a	n/a	n/a	n/a
avg	**-8.48E-01**	**4.77E-02**	**1.22E-02**	**-2.57E-05**

Next, the dynamic model is validated through experimental runs using process parameters in the range used to construct the model. Two process parameter sets, v = 2.6 mm/s and ω = 1600 rpm, and v = 2.18 mm/s and ω = 1810 rpm, are selected for use in validation experiments due to minimal observable flash. Figure 4 shows the axial force measurements taken from varying the plunge depth in a sinusoid manner with a frequency of 0.2 Hz.

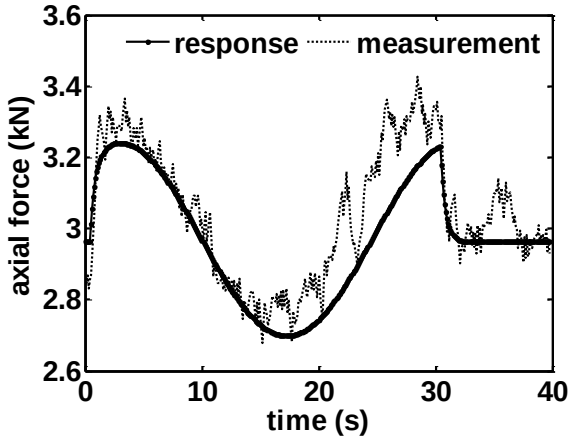

Figure 4. Model Validation Run 1 with v = 2.6 mm/s and ω = 1600 rpm.

The maximum error is approximately 6%. Figure 5 shows the axial force measurements taken from varying the plunge depth in a triangular manner at a frequency of 0.1 Hz.

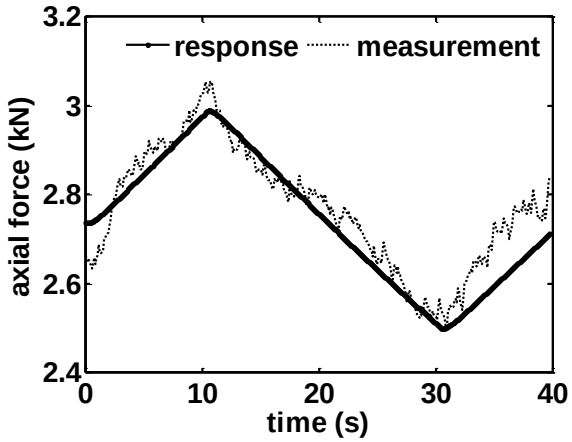

Figure 5. Model Validation Run 2 with v = 2.18 mm/s and ω = 1810 rpm.

The maximum error is approximately 4%. Unlike the previous experiment, the error appears as more evenly distributed about zero. These frequencies of 0.2 Hz and 0.1 Hz were chosen based on operator experience due to rate limits imposed on the plunge depth.

IV. CONTROLLER DESIGN

In this section a controller is designed to regulate the axial force signal. A general tracking controller with constant disturbance rejection is selected and tuned to allow the system to robustly track any desired reference force. General tracking control is a method of combination feed–forward feedback control that theoretically guarantees proper tracking regardless of the reference axial force. The constant disturbance rejection is

necessary due to process repeatability issues (i.e., machine stiffness) as a basic general tracking controller does not contain integral action. The controller is implemented in a Smith Predictor–Corrector (SPC) Structure to allow the system to properly account for the pure communication delay. If the inherent communication delay is ignored, the system model becomes

$$\frac{F_a(z)}{U(z)} = \frac{b_1 z + b_2}{z^2 + a_1 z + a_2} = \frac{b(z)}{a(z)} \tag{61}$$

The error is

$$E(z) = F_R(z) - F_a(z) \tag{62}$$

where $F_R(z)$ is the reference axial force. Equation (62) is rearranged and substituted into equation (61)

$$v(z)a(z)E(z) = v(z)a(z)R(z) - b(z)U(z) \tag{63}$$

where $v(z)$ is the disturbance generating polynomial

$$v(z) = z - 1 \tag{64}$$

A dummy control variable, $\mu(z)$, is defined as

$$\mu(z) = g(z)E(z) = v(z)a(z)R(z) - b(z)U(z) \tag{65}$$

where $g(z)$ is

$$g(z) = g_1 z^2 + g_2 z + g_3 \tag{66}$$

The coefficients g_1, g_2, and g_3 are chosen to shape the closed–loop error dynamics. The closed–loop characteristic equation is

$$z^3 + (a_1 - 1 - g_1)z^2 + (a_2 - a_1 - g_2)z - a_2 - g_3 = 0 \tag{67}$$

The desired closed–loop system has a pole with a time constant of τ = 300 ms and two poles having a natural frequency of ω_n = 30 rad/s and a damping ratio of ζ = 0.9. These closed–loop poles were determined by trial and error and were found to (1) reduce control signal saturation during the transient portion of the response and (2) reduce the natural frequency and increase the damping ratio to decrease the system overshoot, settling time, and oscillations. The desired closed–loop characteristic equation is

$$z^3 - 1.1076z^2 + 0.2177z - 0.0245 = 0 \tag{68}$$

Comparing equations (67) and (68), g_1 = –0.74, g_2 = 0.6776, and g_3 = –0.0232. The controller is implemented in a SPC structure to account for the system communication delay. A block diagram of the system with the general tracking controller implemented in the SPC structure is shown in Figure 6.

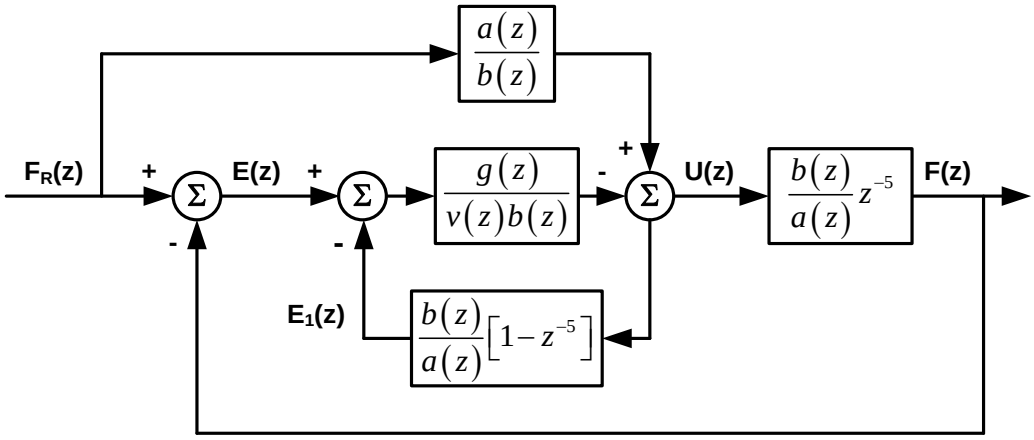

Figure 6. Closed–Loop System Block Diagram with General Tracking Controller in SPC Structure.

The signal $E_1(z)$ is

$$E_1(z) = \frac{b(z)}{a(z)}\left[1 - z^{-5}\right]U(z) \tag{69}$$

Transforming equation (69) into the difference domain

$$\begin{aligned} e_1(k) = &-a_1 e_1(k-1) - a_2 e_1(k-2) \\ &+ b_1\left[u(k-1) - u(k-1-5)\right] \\ &+ b_2\left[u(k-2) - u(k-2-5)\right] \end{aligned} \tag{70}$$

Combining equations (63), (65), and (69) and transforming into the difference domain, the control signal is

$$\begin{aligned} u(k) = &\frac{b_2 - b_1}{b_1}u(k-1) - \frac{b_2}{b_1}u(k-2) + \\ &r(k+1) + \frac{a_1 - 1}{b_1}r(k) + \frac{a_2 - a_1}{b_1}r(k-1) - \\ &\frac{a_2}{b_1}r(k-2) - \frac{g_1}{b_1}\left[e(k) - e_1(k)\right] - \\ &\frac{g_2}{b_1}\left[e(k-1) - e_1(k-1)\right] - \\ &\frac{g_3}{b_1}\left[e(k-2) - e_1(k-2)\right] \end{aligned} \tag{71}$$

V. EXPERIMENTAL STUDIES

In this section, a series of bead–on–plate experiments are conducted to validate the general tracking controller. The traverse rate and spindle rotation speed are constant during each experimental run and saturation limits are imposed on the plunge depth between 4.17 mm and 4.8 mm to ensure that the tool maintains proper contact with the part. A rate limit on the plunge depth is set at ±0.5 mm/s to prevent tool breakage. Two runs have reference force signals consisting of a series of step changes, and one run

contains a sinusoid reference. The reference force signal magnitudes are selected to utilize a significant portion of the plunge depth range.

The results for an experiment with a constant reference force of 3.7 kN are shown in Figure 7.

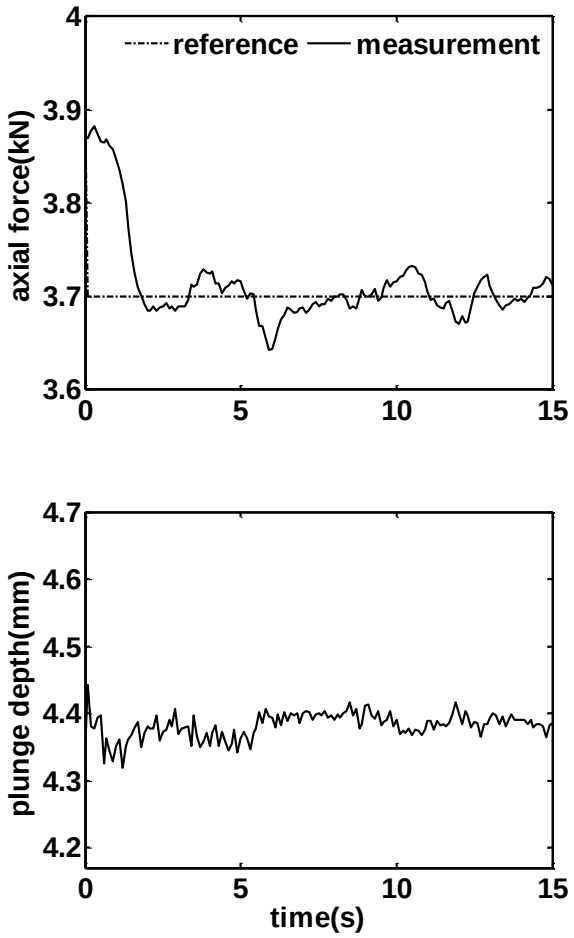

Figure 7. Controller Validation Run 1 with v = 2.18 mm/s and ω = 1810 rpm.

The standard deviation is 48.1 N, 1.23% of the reference. The second run is conducted by varying the reference axial force in a step–wise manner over a range of different inputs. These results are shown in Figure 8.

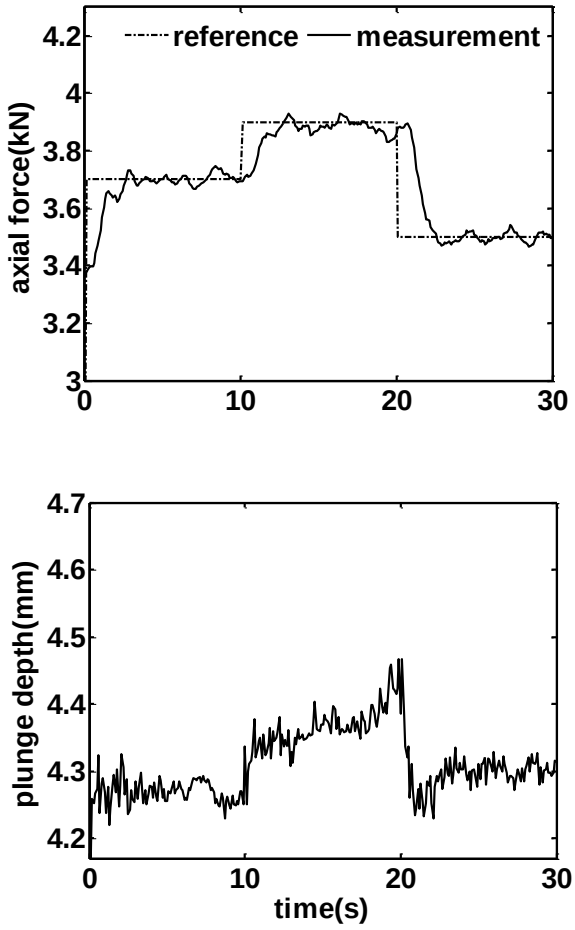

Figure 8. Controller Validation Run 3 with v = 2.6 mm/s and ω = 1600 rpm.

The average standard deviation over this collection of step inputs is 107.2 N, less than 2.89% of the reference force. The results of the third run are shown in Figure 9.

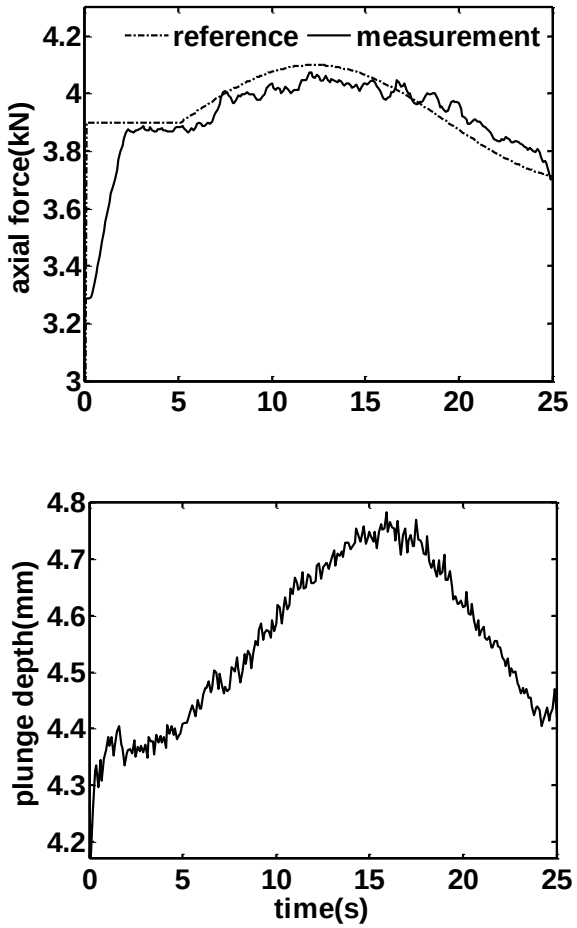

Figure 9. Controller Validation Run 5 with v = 2.18 mm/s and ω = 1810 rpm.

The reference frequency is 0.2 Hz and the average absolute value of the errors is 0.1248 kN.

The control signal for the first constant input run is shown in Figure 7. Note that significant variations are present in the plunge depth to maintain a constant reference force. These variations are due to machine geometric errors, imperfection of the fixturing method, changes in the thermal boundary conditions as the tool advances along the weld path and a number of other factors. The general tracking controller provides an effective

means to compensate for these errors and successfully track a number of desired reference forces.

VI. SUMMARY AND CONCLUSIONS

Empirical models were constructed from a series of experiments do determine steady–state and dynamic relationships between the input process parameters and the axial force for use in controller design for Friction Stir Welding processes. Following model validation, a general tracking controller with disturbance rejection was designed to robustly track a variety of desired reference axial forces with zero steady–state error. The controller was implemented in a Smith Predictor–Corrector structure to account for an inherent communication delay in the FSW system due to the method of controller interrupt.

The controller was validated through a collection of step tests and sinusoid references to demonstrate the ability to track non–constant references. The experimental results demonstrate excellent tracking of all reference signals with minimal error most likely due to the physical limitations of the process (i.e., rate limit due to material stiffness). The standard deviation of the controlled response was found to be approximately one percent of the reference signal magnitude.

VII. REFERENCES

Cederqvist, L., Bolmsjo, G., and Sorensen, C., 2007, “Adaptive Control of Novel Welding Process to Seal Canisters Containing Sweden’s Nuclear Waste Using PID Algorithms,” Lunds University.

Kalya, P., 2008, Modeling and Control of Friction Stir Welding, Doctoral Dissertation, Mechanical and Aerospace Engineering Department, Missouri University of Science and Technology.

Zhao, X., Kalya, P., Landers, R.G., and Krishnamurthy, K., 2007, "Design and Implementation of a Nonlinear Axial Force Controller for Friction Stir Welding Processes," *American Control Conference*, New York, New York, July 11–13.

SECTION

2. SUMMARY, CONCLUSIONS, AND FUTURE WORK

A method of stochastic modeling is introduced and used for the model update stage of a two-step Kalman filter. The filtering methodology is applied to model and control both Friction Stir Welding and Laser Metal Deposition processes. Values of λ and Q are tuned to significantly reduce the signal variance for both cases. The experimental results demonstrate the ability of the filtering methodology to reduce the axial force and temperature signal variances by an order of magnitude, while preserving the original trends of the data.

A series of bead-on-plate welds are conducted in a Friction Stir Welding process to develop static and dynamic models relating the input process parameters to the axial force signals. The models are used in conjunction with a Smith Predictor-Corrector Structure to design and implement a general tracking controller with disturbance rejection for online control of the axial force signals. The controller is experimentally validated through a series of step and sinusoid changes in the reference axial force signal. The second order model is an adequate approximation for the Friction Stir Welding process. Any errors in the combined equipment and process dynamics model are sufficiently suppressed by the addition of disturbance rejection (integral control) to the general tracking controller.

Future work on the filtering method involves the addition of an input term to reduce the delay in estimate response due to changes in the input. The Friction Stir Welding work needs to be expanded to lap and butt welds. Complex reference force signals must be investigated to accommodate the nonlinear velocity profiles required for corner welding.

BIBLIOGRAPHY

[1] Smith, C.B., Hinrichs, J.F., and Crusan, W.A., 2003, "Robotic Friction Stir Welding: the State of the Art," *Proceedings of the* 4th *International Symposium of Friction Stir Welding*, Park City, Utah, May 14–16.

[2] Kalya, P., 2007, *Modeling and Control of Friction Stir Welding*, Doctoral Dissertation, University of Missouri–Rolla, Department of Mechanical and Aerospace Engineering, Rolla, Missouri.

[3] Zhao, X., Kalya, P., Landers, R.G., and Krishnamurthy, K., 2007, "Empirical Dynamic Modeling of Friction Stir Welding Processes," *ASME International Conference on Manufacturing Science and Engineering*, Atlanta, Georgia, October 15–18.

[4] Zhao, X., Kalya, P., Landers, R.G., and Krishnamurthy, K., 2007, "Design and Implementation of a Nonlinear Axial Force Controller for Friction Stir Welding Processes," *American Control Conference*, New York, New York, July 11–13.

VITA

Thomas M. Oakes was born in Jefferson City, MO, on October 18, 1984. He graduated from Helias High School in 2003 and moved to Rolla, MO to attend the University of Missouri. Thomas received his Bachelor of Science in Mechanical Engineering in December of 2007 and continued his education at Missouri University of Science and Technology (formerly UMR). He received his Master of Science in Mechanical Engineering in December of 2009 and applied for the Nuclear Engineering program at the University of Missouri in Columbia for a doctorate.

Thomas has been a member of Kappa Mu Epsilon, the math honor fraternity as well as Pi Tau Sigma, the Mechanical Engineering honor fraternity. He has published a book chapter in Kalman Filtering in Manufacturing and presented his welding research at the 2009 American Controls Conference.